

Observed variability of the West India Coastal Current on the continental slope from 2009–2018

Anya Chaudhuri¹, D. Shankar^{1,*}, S. G. Aparna¹, P. Amol², V. Fernando¹,
A. Kankonkar¹, G. S. Michael¹, N. P. Satelkar¹, S. T. Khalap¹, A. P. Tari¹,
M. G. Gaonkar¹, S. Ghatkar¹, and R. R. Khedekar¹

¹CSIR-National Institute of Oceanography, Dona Paula, Goa 403004, India

²CSIR-National Institute of Oceanography Regional Centre, Visakhapatnam, India

*Corresponding author: shankar@nio.org

October 21, 2019

Abstract

We describe the variability of the West India Coastal Current (WICC) during October 2008 to October 2018 using data from ADCP (acoustic Doppler current profiler) moorings deployed on the continental slope off the west coast of India. The four moorings are deployed off Mumbai ($\sim 20^\circ\text{N}$), Goa ($\sim 15^\circ\text{N}$), Kollam ($\sim 9^\circ\text{N}$), and Kanyakumari ($\sim 7^\circ\text{N}$). This 10-year data set allows us to attach a statistical significance to the conclusions drawn by Amol et al. (2014) on the basis of four years (October 2008 to October 2012) of ADCP data. The longer data set confirms the earlier finding that intraseasonal variability in the 30–90-day band dominates the variability of the WICC at all locations and that this intraseasonal variability peaks during the winter monsoon. The annual cycle (300–400 days) is strong and statistically significant at all locations. The phase propagates upward for the annual cycle and this phase difference is seen in the relative phases of both, the ADCP currents at 25 m and 48 m as well as the 48 m ADCP and satellite-derived currents. The intra-annual (100–250 days) and intraseasonal currents show instances of both upward and downward phase propagation. The alongshore wavelet coherence is high on seasonal time scales between adjacent mooring locations and several instances of high coherence are seen even on intraseasonal timescales. Data gaps off Goa and Kanyakumari restrict the significant wavelet power to the ADCP records off Kollam and Mumbai, and the coherence analysis shows that the WICC off Kollam leads Mumbai on seasonal scales. The direction of the alongshore WICC is, however, largely determined by the direction of the significantly larger intraseasonal component. Though the climatological seasonal cycle over the whole record does show the canonical equatorward flow during the summer monsoon (June–September) and poleward flow during the winter monsoon (November–February), the scatter around the daily mean is very high. The data show that the WICC may flow in either direction on a given day of the year, with this unpredictability of direction being stronger off Kollam, where the $1\text{-}\sigma$ band of the daily mean alongshore WICC shows that it can flow in either direction in most months. The seasonality is stronger off Mumbai, where the width of the $1\text{-}\sigma$ band is less. The decade-long continuous record off Kollam and Mumbai shows that the sub-annual alongshore WICC at both locations is significant and is comparable to or stronger than the annual component. The cross-shore sub-annual current is also strong off Kollam and is seen to be associated with eddy-like circulations.

Eastern boundary currents; ADCP; Seasonal variability; Intraseasonal variability; Interannual variability; WICC; Arabian Sea; Indian Ocean.

1 Introduction

The West India Coastal Current (WICC) is the eastern-boundary current of the Arabian Sea. Its climatological seasonal cycle, inferred from ship drifts and altimetry (Shetye and Shenoi, 1988; Shankar and Shetye, 1997; Shetye and Gouveia, 1998; Shetye, 1998; Shankar, 2000; Schott and McCreary, 2001; Shankar et al., 2002), shows a seasonally reversing surface current flowing poleward during the winter monsoon (November–February) and equatorward during the summer monsoon (June–September). The alongshore component of the monthly-mean winds along the west coast of India is equatorward throughout the year, implying that the poleward WICC in winter flows into the wind (Johannessen et al., 1987; Shetye and Shenoi, 1988; Shetye et al., 1991b).

While ship drifts and altimeter-based sea-level data can help map the surface currents, hydrography and direct current measurements are necessary to estimate the sub-surface currents. A set of cruises along the Indian west coast (Shetye et al., 1990, 1991b) and east coast (Shetye et al., 1991a, 1993, 1996) mapped the WICC and EICC, respectively, enabling investigation of the dynamics of these boundary currents. The hydrographic data show that the core of the WICC lies on the continental slope roughly along the 1000 m isobath and the current extends up to a depth of ~ 150 –200 m, below which the isopycnals reverse, suggesting the existence of an undercurrent (Shetye et al., 1990, 1991b).

As described by Amol et al. (2014), these hydrographic cruises enabled the development of a theoretical framework that ties the dynamics of the WICC and EICC to the basin-scale dynamics of the Indian Ocean. This theoretical framework for the seasonal circulation of the WICC incorporates the effect of Kelvin waves that are forced along the east coast of India (McCreary et al., 1993; Shankar and Shetye, 1997; Shankar et al., 2002). These Kelvin waves set up an alongshore pressure gradient along the Indian west coast and this pressure gradient overwhelms the wind forcing, allowing the WICC to flow into the wind (McCreary et al., 1993). Model studies show that these remotely forced Kelvin waves are more important for the seasonal cycle of the WICC than the local west-coast winds (Shankar and Shetye, 1997; Shankar et al., 2002).

Yet, in spite of the theoretical developments, studies of the WICC were limited largely to the seasonal cycle owing to the lack of data, other than from satellite altimetry, that could resolve the intraseasonal variability. The dearth of direct current measurements precluded quantification of the intraseasonal variability of the WICC, prompting the CSIR-National Institute of Oceanography to launch a programme under which moorings equipped with acoustic Doppler current profilers (ADCPs) were deployed on the continental slope and shelf off the Indian west (Amol et al., 2014) and east (Mukherjee et al., 2014) coasts. The first description of the slope currents from these ADCP moorings was by Vialard et al. (2009), who noted that intraseasonal variability dominated the upper-ocean currents off Goa (see Fig. 1). Vialard et al. (2009) attributed this dominance of intraseasonal variability to the coastal trapping of the intraseasonal currents. Amol et al. (2012) used the ADCP data during March–September 2008 from three moorings off the central west coast of India to document the existence of coastally-trapped waves (CTWs), providing observational evidence for the existence of remote forcing of the WICC.

Amol et al. (2014) used the ADCP data from four mooring locations (see Fig. 1) during 2008–2012 to

quantify the seasonal and intraseasonal variability of the WICC on the continental slope. Their analysis shows that intraseasonal variability is stronger than the seasonal variability and it peaks during the winter monsoon. The seasonal cycle shows significant interannual variability even within this limited 4-year period. The annual cycle, whose amplitude increases poleward, shows upward phase propagation, leading to a shallowing of the undercurrent with time. The seasonal WICC is weakly correlated along the coast, but the intraseasonal WICC is decorrelated. While the cross-shore current is weak at the northern moorings off Mumbai and Goa, it is significant off Kollam and Kanyakumari in the south.

The mooring programme continues to date and we use a decade-long ADCP data set (2008–2018) to describe the variability of the WICC. This paper is therefore a sequel to Amol et al. (2014, A14 henceforth). This longer data set confirms several of the results reported by A14, but also shows some new features. At all four mooring locations (off Kanyakumari, Kollam, Goa, and Mumbai), intraseasonal variability is stronger than the seasonal cycle. While the climatological seasonal cycle matches the canonical equatorward flow during the summer monsoon and poleward flow during the winter monsoon, it is seen that the direction of the WICC on a given day of the year is largely unpredictable due to this dominance of the intraseasonal component. Data gaps off Goa and Kanyakumari restrict the description of the lower frequencies to the moorings off Kollam and Mumbai, for which the annual cycle is statistically within the cone of influence in a wavelet analysis. The annual cycle off Mumbai shows upward phase propagation throughout, but both upward and downward propagation of phase are seen in the intra-annual and intraseasonal bands. The longer data set also suggests the presence of significant sub-annual variability in the regime of the WICC; the sub-annual alongshore WICC is strong and poleward off Kollam.

We start with a description of the data and methods of analysis in Section 2. An overview of the sub-inertial alongshore and cross-shore WICC in Section 3 is followed by a more detailed description of the seasonal cycle in Section 4 and intraseasonal and interannual variability in Section 5. Section 6 concludes the paper.

2 Data and methods

Our primary data are from four ADCP moorings off the Indian west coast, but we use four additional data sets.

2.1 ADCP data

The four ADCP moorings located roughly on the 1000–1100 m isobath along the continental slope off Mumbai ($\sim 20^\circ\text{N}$), Goa ($\sim 15^\circ\text{N}$), Kollam ($\sim 9^\circ\text{N}$), and Kanyakumari ($\sim 7^\circ\text{N}$). The availability of data at these four locations varies with time and there are several gaps off Goa and Kanyakumari, but a long and continuous time series is available off Mumbai and Kollam. The mooring and ADCP details are given in Tables 1–4 for Mumbai, Goa, Kollam, and Kanyakumari, respectively.

The mooring configuration has changed as the programme evolved over time. In the first few years of the time series, when only one ~ 76 kHz ADCP was deployed on a mooring line, the shallowest depth for current measurements is ~ 40 m (Tables 1–4; A14). In later years, however, the use of 153 kHz ADCPs shifted up the shallowest ADCP bin to ~ 20 m. The measurements are available hourly at a depth

resolution of 8 m for the 76 kHz ADCPs and 4 m for the 153 kHz and 307 kHz ADCPs. Most of the ADCPs on these moorings are upward-looking, but downward-looking 307 kHz ADCPs were deployed twice during 2011–2012 off Goa (Table 2) and once during the same period off Kanyakumari (Table 4).

The method of data processing is essentially as described by A14, but there are three differences. Following A14, the entire time series is detided using the Tidal Analysis Software Kit (TASK; Bell et al., 1998) after the initial processing of the current data. The de-tided currents below ~ 200 m are then rotated to retrieve the alongshore and sub-inertial cross-shore components: a least-square approach is used to minimise the sub-inertial cross-shore component. The depth interpolation follows Kutsuwada and McPhaden (2002); this method, based on regression relations and data from adjacent depths, incorporates the information from two adjacent depth bins on either side.

The time interpolation is done using the grafting method of Mukhopadhyay et al. (2017) because this method gives more accuracy compared to linear interpolation when the gaps extend beyond ~ 12 hours; this is the first difference between the method used in this paper and in A14.

Since the inertial period off Mumbai (Kanyakumari) is ~ 2 days (~ 4 days), the currents are filtered with a 5-day low-pass filter to obtain the sub-inertial currents (A14). A band-pass Lanczos filter is then used to extract the annual (300–400-days band-pass) and intra-annual (100–250-days band-pass) cycles, which together constitute the seasonal cycle, and the variability at intraseasonal periods (30–90-days band-pass). The use of the Lanczos filter in preference to the Butterworth filter is the second difference from A14.

The response of the Lanczos low-pass filter around the cutoff frequency falls from 1 to 0 over a finite transition width. This width is inversely proportional to the number of weights that is used in the filter. For a band-pass filter, with cutoff frequencies f_1 and f_2 ($f_1 > f_2$), there is a finite width over which the response tapers at f_1 and at f_2 ; if the two bands overlap, then the response even in the centre of the band never reaches 1 and is attenuated (Duchon, 1979). Increasing the weights increases the response in the centre of the band. The number of weights required increases inversely with the difference $f_1 - f_2$. While the choice of weights does not matter for the intraseasonal band, it does matter for the annual cycle because the number of weights required can involve the loss of several years of data near the end of the time series for sufficiently small values of $f_1 - f_2$. This effect is prominent for the annual and sub-annual components. We have chosen a weighting window of about $3/f_2$, where f_2 is the lower frequency (in the units of the time interval used for the analysis). We note, however, that even with this large window size, there is an attenuation of the annual and sub-annual signals and our estimate may therefore be considered the lower bound for the actual annual or sub-annual signals. A similar problem occurs with the Butterworth filter, but its effect varies over the time series. The Lanczos filter with the above choice of weights matches the response of the Butterworth filter. The loss of data due to a finite window size of the Lanczos filter occurs near the ends of the time series (or near the edges of data gaps), which corresponds to the region in which the response of the Butterworth filter is distorted.

The third difference from A14 is in the correction applied for a change in transducer depth. A14 did not apply this correction, but we find that there are large changes in the depth of the ADCP transducer over short durations. These variations in the depth of a transducer, mostly due to sub-surface currents, leads to a change in the depth of observation with time for a given distance from the ADCP. Hence, the actual depth of observation needs to be calculated at every time step in order to accurately map the currents.

The correct depth for a measurement in a particular bin, say n , at a given time t is given by

$$D_{\text{ob}}(n, t) = D_A(t) - D_{\text{bin}}(n), \quad (1)$$

for upward-looking ADCPs and

$$D_{\text{ob}}(n, t) = D_A(t) + D_{\text{bin}}(n) \quad (2)$$

for downward-looking ADCPs, where $D_A(t)$ is the depth of the ADCP transducer and it changes with time. $D_{\text{bin}}(n)$ is the distance of the observation bin from the ADCP and depends only on the bin size and bin number (n). $D_{\text{ob}}(n, t)$ therefore depends on both the bin number and the time. The bin size, as noted earlier is 8 m (4 m) for the ~ 76 kHz (~ 153 and ~ 307 kHz) ADCPs. Hence, the same bin number would translate into different depths of observations, due to which there would be some gaps in the data at shallower depths.

Though this re-mapping is important for accurate current maps, it must be noted that the depth fluctuations are negligible (< 10 m) over most of the record. Off Goa, there is an excursion of ~ 150 m during 2013–2014 (ADCP G9A in Table 2) and there are a few similar, but short-lived, excursions off Kanyakumari. The largest excursions (~ 195 m) occur off Kanyakumari during 2016 (ADCPs KK6A and KK6B in Table 4). A comparison of the uncorrected and corrected alongshore current at 100 m off Kanyakumari shows the large movement during 30 June to 5 July 2016 (Fig. 2). In spite of the large excursion, its short duration implies that the effect on the sub-inertial current is negligible.

In the rest of this paper, the basic data set consists of the sub-inertial, rotated (alongshore and cross-shore) currents estimated from the ADCP data.

The tool we use for analysis is the wavelet power spectrum. Unlike a Fourier spectrum, which is appropriate for a stationary time series, the wavelet power spectrum allows the determination of the power at different time scales and also information on how this power evolves with time; this information is useful for a non-stationary time series (Torrence and Compo, 1998). The Morlet wavelet spectra have been used here (as in A14) to describe the variation of the intraseasonal and seasonal WICC with time. Edge effects distort the spectrum that lies outside the cone of influence, limiting the potential of shorter time series available to A14; the decade-long record used in this paper brings more periodicities within the cone of influence of the wavelet spectrum.

Likewise, the wavelet coherence can be used to obtain the coherence between the wavelets for two different time series at different time scales as a function of time. The wavelet cross-spectrum between wavelets for two time series, $W_i^x(s)$ and $W_i^y(s)$, is the expectation value of the product of these two quantities, $\langle W_i^x(s) W_i^y(s)^* \rangle$, where i is a particular time and s is the time scale. The wavelet coherence is the normalised wavelet cross-spectrum and ranges in values between 0 and 1 (Maraun and Kurths, 2004). The calculation of the wavelet coherence requires smoothing in time and scale to calculate the expectation value. The wavelet coherence was calculated using the wavelet coherence R package SOWAS (Maraun and Kurths, 2004; Maraun et al., 2007).

2.2 Other data sets

The other data sets we use include altimeter sea-level anomalies (SLAs) from AVISO (1996) and the OSCAR (Ocean Surface Currents Analyses Real-time) data product for near-surface currents (Bonjean

and Lagerloef, 2002). OSCAR is an ocean-surface-current data product for the global ocean from 1992 onwards and data are available on both $1^\circ \times 1^\circ$ and $0.333^\circ \times 0.333^\circ$ grids every 5 days. The OSCAR current, derived from satellite measurements of SLA, winds, and sea-surface temperature (SST) using the geostrophic, Ekman-Stommel, and thermal-wind relations, represents the average current over the top ~ 30 m and has been shown to match the direct current measurements well in the eastern Arabian Sea (A14) and the western (Mukherjee et al., 2014) and eastern (Sikhakolli et al., 2013) Bay of Bengal. We use the OSCAR data on the finer, $0.333^\circ \times 0.333^\circ$, grid.

In addition, we validate two model-based products that are popularly used for studying the circulation: these products are the ECCO2 (Estimating the Circulation and Climate of the Ocean, Phase 2) state estimate Menemenlis et al. (2008) and the HyCOM (Hybrid Coordinate ocean Model; Chassignet et al., 2007) reanalysis. The ECCO2 state is obtained by making optimal adjustment of model parameters, initial conditions, and boundary conditions through a series of sensitivity numerical simulations and minimisation of model-observation misfit. The optimised model solution, called Cube92, is provided as an interpolated product on a $0.25^\circ \times 0.25^\circ$ grid (ftp://ecco.jpl.nasa.gov/ECCO2/cube92_latlon_quart_90S90N/). The ECCO2 grid points closest to the ADCP data locations off Mumbai, Goa, Kollam, and Kanyakumari are at $(69.125^\circ\text{E}, 19.875^\circ\text{N})$, $(72.625^\circ\text{E}, 15.125^\circ\text{N})$, $(75.375^\circ\text{E}, 8.875^\circ\text{N})$, and $(77.375^\circ\text{E}, 6.875^\circ\text{N})$, respectively. The HyCOM reanalysis is a gridded product based on HyCOM and the Navy Coupled Ocean Data Assimilation (NCODA). It has a horizontal resolution of 0.08° between 40°S and 40°N and 0.04° poleward of these latitudes. This data set is available only from 1994 to 2015 (<https://hycom.org/dataserver/gofs-3pt1/reanalysis>); hence, we compare it to the ADCP currents only up to 2015. The HyCOM grid points closest to the ADCP data locations off Mumbai, Goa, Kollam and Kanyakumari are located at $(69.28^\circ\text{E}, 20^\circ\text{N})$, $(72.72^\circ\text{E}, 15.12^\circ\text{N})$, $(75.36^\circ\text{E}, 8.96^\circ\text{N})$, and $(77.36^\circ\text{E}, 6.96^\circ\text{N})$, respectively.

3 The sub-inertial WICC

Since the top (bottom) ADCP bin for which data are available throughout the time series at all locations is at 48 m (300 m), most of the analysis is restricted to the top 300 m. Whenever a 153 kHz ADCP was available at depths shallower than ~ 200 m, the sub-inertial current is available closer to the surface (up to ~ 24 m). The sub-inertial alongshore and cross-shore components are discussed in this section. For convenience and consistency with the literature, we refer to summer monsoon (June–September) and winter monsoon (November–February) while discussing the variability; October and March–May represent the transition between these two seasons.

3.1 Alongshore component

Strong intraseasonal variability is evident in the sub-inertial alongshore WICC at all four mooring locations: the current reverses often and, as noted by A14, such reversals are common even within a season (Fig. 3). Off Mumbai, Goa, and Kollam, the current weakens with depth and often changes direction below ~ 150 – 200 m, suggesting the existence of an undercurrent, but the alongshore current is deeper off Kanyakumari.

The variability with respect to time can be ascertained using a wavelet analysis. Following A14, we

split the seasonal cycle into an annual cycle, which has a period around ~ 365 days, and intra-annual variability, which consists of the semi-annual cycle (period ~ 180 days) and a band around 120 days. Notwithstanding the data gaps off Goa and Kanyakumari, the longer data record leads to the annual cycle lying within the cone of influence of the wavelet spectrum over a part of the record, implying that it is statistically reliable. The normalisation in our wavelet analysis follows Torrence and Compo (1998), whose method leads to a flat white-noise spectrum, but implies that sine functions of equal amplitude will exhibit different integrated powers proportional to their oscillation scale (Maraun and Kurths, 2004). In other words, while it is possible to compare the variability over time within a specific period band, it is not possible to compare the wavelet power across period bands because the normalisation emphasises the wavelet power at higher periods: the same wavelet power at a higher period would imply lower variability compared to a lower period. Hence, though the wavelet analysis suggests a seasonal cycle comparable to or stronger than intraseasonal variability at all four locations (Fig. 4), analysis of the filtered currents shows that the annual current is weaker than the intra-annual current and both these components of the seasonal cycle are weaker than the intraseasonal current during the winter monsoon. We discuss the variability in the seasonal and intraseasonal bands in Sections 4 and 5.1, respectively.

A14 noted that except off Kollam, the annual mean near-surface current did not exceed 4 cm s^{-1} . The annual-mean current off Mumbai and Kanyakumari lies within 5 cm s^{-1} for all years even in the longer data set, but its value is $\sim 8 \text{ cm s}^{-1}$ off Goa during 2017. Off Kollam, as noted by A14, the near-surface, annual-mean current is generally poleward; the only exception during 2008–2018 is 2012. The annual-mean current off Kollam current peaks around 60–100 m and the value is $\sim 6\text{--}10 \text{ cm s}^{-1}$ in some years.

A wavelet-coherence analysis of the ADCP current at 48 m with the OSCAR current shows high coherence (correlation exceeding 0.65) at all four locations; the coherence is high, even if patchy, even in the intraseasonal band (Fig. 5). In the OSCAR data set used here, the grid points closest to the ADCP moorings off Mumbai, Goa, Kollam, and Kanyakumari are at $(69.3^\circ\text{E}, 20^\circ\text{N})$, $(72.7^\circ\text{E}, 15^\circ\text{N})$, $(75.3^\circ\text{E}, 9^\circ\text{N})$, and $(77.3^\circ\text{E}, 7^\circ\text{N})$, respectively. The high correlation off Kollam is in contrast to the low correlation obtained by A14, but their OSCAR cell was located $\sim 1^\circ$ away from the ADCP location. For the seasonal cycle at all locations, the ADCP current at 48 m leads the OSCAR current, which represents the current averaged over 0–30 m, in accordance with the upward phase propagation noted by A14. The phase difference is highest off Kollam (Fig. 5).

The use of 153 kHz ADCPs at the top of the mooring line after 2012 implies the availability of ADCP data within the top 30 m. These data are available off Mumbai (Table 1), Goa (Table 2), and Kollam (Table 3), but data gaps do not permit a similar analysis off Kanyakumari (Table 4). A wavelet-coherence analysis shows high coherence for the seasonal cycle between the ADCP currents at 48 m and 25 m (Fig. 6), with the current at 48 m leading. The phase difference, as expected from the comparison between the ADCP current at 48 m and the OSCAR current (Fig. 5), is highest off Kollam.

3.2 Cross-shore component

As noted by A14, the sub-inertial cross-shore current is weak off Mumbai and Goa, where it tends to be stronger during the winter monsoon, and strong off Kollam and Kanyakumari, where it is strong over much of the year (Fig. 7). Like the alongshore component (Fig. 3), the cross-shore component also reverse often within a season, and its strong intraseasonal variability is evident in the wavelet power

spectrum (Fig. 8). The annual cycle is weak off Mumbai and Goa compared to Kollam, but it weakens off Kollam too after 2013. The annual cross-shore component at these two northern locations is much weaker than the annual alongshore component (Fig. 4,8).

At all locations, including Kollam and Kanyakumari, the cross-shore current weakens significantly below ~ 200 m (Fig. 7). A comparison of the 48 m cross-shore current with the OSCAR current shows high coherence off Kollam, Kanyakumari, and Goa, but the coherence is weak off Mumbai (figure not shown).

Off both Kollam and Kanyakumari, there is high wavelet power at periods higher than the annual, but these periods lie outside the cone of influence off Kanyakumari (Fig. 8). We deal with this sub-annual variability in Section 5.2. The intra-annual component of the cross-shore current is also stronger than the intra-annual component of the alongshore current off Kollam in some years (Section 4.2).

4 The seasonal cycle

As noted earlier, the seasonal cycle consists of the annual cycle and intra-annual variability consisting of the semi-annual and 120-day bands. In this section, we filter the alongshore current with band-pass Lanczos filters to quantify the variability in the annual (300–400 days band-pass-filtered) and intra-annual (100–250 days band-pass-filtered) bands.

4.1 The annual cycle

The loss of data owing to gaps makes it difficult to interpret the annual cycle off Goa and Kanyakumari, forcing us to restrict our description for this band to Mumbai and Kollam; the limited data available off Goa and Kanyakumari suggest, however, a similarity in the magnitude of the alongshore current between Mumbai and Goa and Kollam and Kanyakumari (Fig. 9).

The annual cycle is stronger off Mumbai compared to Kollam and upward propagation of phase, noted in the shorter record by A14, is prominent in all years at both locations (Fig. 9). This upward phase propagation in the annual band is evident in the strong wavelet coherence between the OSCAR current and the ADCP current at 48 m, with the latter leading (Fig. 5). The annual alongshore WICC weakens more with depth off Kollam than off Mumbai, where the annual component exceeds 6 cm s^{-1} even at 200 m.

Though the data gaps off Goa and Kanyakumari preclude a statistically robust estimate of the alongshore coherence of the annual component owing to the annual cycle lying outside the cone of influence (Fig. 4), wavelet-coherence analysis does suggest a strong coherence at the annual cycle between the Kanyakumari–Kollam, Kollam–Goa, and Goa–Mumbai pairs, but with the coherence varying over the time series (Fig. 10). This alongshore coherence and its temporal variation is also evident in the wavelet coherence for the annual cycle between Kollam and Mumbai. Though the analysis suggests that the coherence is stronger during 2013–2014 and after 2015, the data do suggest a fairly strong alongshore coherence of the alongshore WICC in the annual band.

4.2 Intra-annual variability

The magnitude of the intra-annual component tends to increase equatorward along the coast, with the intra-annual WICC being weaker than the annual WICC off Mumbai, but stronger off Goa and Kollam; off Kanyakumari, we do not have sufficient information on the annual component to draw an inference (Fig. 9). The strength of the intra-annual component (Fig. 9) and the variability in this band (Fig. 4) change with time. For example, off Mumbai, the intra-annual component is strongest during 2014, when the variability is more semi-annual, and 2016, when the variability is seen around the 120-day band (Fig. 4); accordingly, the current at 48 m shows more reversals during 2016 compared to 2014 (Fig. 9). The intra-annual current (Fig. 9) and intra-annual variability (Fig. 4) are also strong off Kollam during these two years, but the switch from the semi-annual band to the 120-day band is not seen at this location. Off Kollam, the intra-annual band is also strong during 2011–2012. Unlike A14, however, we do not find the strong intra-annual variability limited to the winter monsoon: it is strong during the summer monsoon as well, with examples being seen during 2014 off Mumbai and Kollam and during 2016 off Goa and Kollam (Fig. 9).

While upward propagation of phase is evident in the intra-annual band as well (Fig. 9), downward propagation of phase is also seen in some years: examples include 2010 off Mumbai and Goa, 2014–2015 off Kollam, and 2016 off Mumbai and Kollam. In some years, this change in the direction of phase propagation can be seen in the switch in phase lag between the OSCAR and 48 m ADCP current (Fig. 5) or the ADCP currents at 48 m and 24 m (Fig. 6).

A14 noted a higher alongshore coherence between Kollam and Goa compared to Goa and Mumbai; this higher coherence between Kollam and Goa is evident for this band during 2011 (Fig. 10). The coherence between Kollam and Goa is high again during 2016, but the coherence between Goa and Mumbai and Kanyakumari and Kollam is also high during 2016–2017. As noted by A14 and seen in Fig. 10, Kollam leads Kanyakumari at ~ 110 days during February–March 2013, when the coherence at 48 m is high between these locations; during the summer monsoon of 2016 and February–July 2017, however, when the coherence between these locations peaks again, Kollam tends to lag Kanyakumari. Between Kollam and Mumbai, however, the coherence in this band is weak, unlike for the annual band (Fig. 10).

Off Kollam, the cross-shore component is often stronger than the alongshore component in the intra-annual band. An example is seen during March 2013 (Fig. 11), when the cross-shore peak in this band is $\sim 16 \text{ cm s}^{-1}$ (offshore) compared to the alongshore peak of $\sim 8 \text{ cm s}^{-1}$ (equatorward). This strong cross-shore flow is also seen in the OSCAR current and is associated with the quasi-geostrophic flow around an eddy in the southeastern Arabian Sea (Fig. 11). Such strong cross-shore flows are seen on a few other occasions too off Kollam in the intra-annual band, but not in the annual band.

5 Intraseasonal and interannual variability

Deviations from the seasonal cycle occur due to variability at intraseasonal and interannual periods, which we quantify in this section.

5.1 Intraseasonal variability

As noted by A14 for 2008–2012, variability of the alongshore WICC in the 30–90-day intraseasonal band is strong at all four locations in all years (Fig. 4). The intraseasonal component of the current (Fig. 12) is stronger than the annual and intra-annual components (Fig. 9). Though the intraseasonal component tends to peak during the winter monsoon, as noted by A14, the intraseasonal WICC is strong during the summer monsoon of 2013 (2016 and 2017) off Kollam (Kanyakumari; Fig. 12). In the 4–30-day band, however, the strong intraseasonal currents are restricted largely to the winter monsoon (Fig. 4).

Off Kanyakumari, unlike at the other three locations, the strong intraseasonal current in the 30–90-day band extends below 300 m (Fig. 12). Zooming into the time-depth plot of the alongshore WICC shows that the phase propagates both upward and downward in this intraseasonal band at all four locations. There is high coherence in the 30–90 day band between the 48 m ADCP current and the OSCAR current (Fig. 5) and between the 48 m and 24 m ADCP currents (Fig. 6). The coherence is low, however, in the 4–30-day band, with high values occurring in patches. As noted by A14, the alongshore coherence weakens for the intraseasonal band (Fig. 10), but it is high in patches between adjacent mooring pairs (Kanyakumari–Kollam, Kollam–Goa, and Goa–Mumbai) and between Kollam and Mumbai (Fig. 10).

5.2 Sub-annual variability

The longer record permits a description of the variability at sub-annual periods, to obtain which we use a 500-day low-pass Lanczos filter. The sub-annual alongshore WICC off Mumbai and Kollam (Fig. 13) is comparable to the its annual component (Fig. 9). Off Mumbai, the sub-annual alongshore WICC has a peak value of $\sim 4 \text{ cm s}^{-1}$ during 2011 (equatorward) and 2015 (poleward; Fig. 13). Off Kollam, the sub-annual current is largely poleward and the peak value exceeds 10 cm s^{-1} during 2014; the sub-annual WICC off Kollam flows equatorward only between November 2011 to June 2012 and the peak value of $\sim 4 \text{ cm s}^{-1}$ is much weaker than the poleward flow during the rest of the time series. That’s why, as noted by A14, the annual mean alongshore WICC tends to flow poleward in most years, but is equatorward during 2012. The coherence between the ADCP current at 48 m and the OSCAR current is high even in this sub-annual regime off Mumbai (Fig. 5); though the coherence is weaker off Kollam, the two estimates still match well in some years (Figs. 5,13). The strong sub-annual flow extends to $\sim 150 \text{ m}$ off both Mumbai and Kollam and there is clear evidence for an undercurrent when this sub-annual component weakens (Fig. 13).

The cross-shore component of the sub-annual WICC is weaker than its alongshore counterpart off Mumbai, but the two components are comparable off Kollam (Fig. 13). As seen earlier for the intra-annual band (Fig. 11), these strong cross-shore flows in the sub-annual regime are associated with eddy-like circulations (Fig. 14).

6 Discussion

We have used ADCP measurements from the continental slope off the Indian west coast at four locations — Mumbai, Goa, Kollam, and Kanyakumari — to analyse the variability of the WICC on time scales ranging from intraseasonal to sub-annual. The time period of the ADCP measurements used here is

October 2008 to October 2018 and our analysis of this decade-long record is therefore a sequel to A14, who used a shorter data set (2008–2012) to present the first quantitative description of the variability of the WICC on time scales ranging from the intraseasonal to seasonal. The longer record ensures that the annual cycle lies within the cone of influence of a wavelet transform for several years (Figs. 4,8), implying that the results presented here are statistically more robust than the results of A14. The longer data set allows us to confirm some of the results of A14, but also shows some new features and permits an analysis of sub-annual variability.

A prominent annual cycle is seen at all four locations, including Kanyakumari (Figs. 4,9) where A14 did not find significant wavelet power in the annual band. Off Mumbai and Kollam, where data gaps (Tables 1,3) do not affect the analysis as off Goa and Kanyakumari (Tables 2,4), the upward propagation of phase noted by A14 is evident throughout the record for the annual cycle (Fig. 9). While upward propagation of phase is also seen at intra-annual (Fig. 9) and intraseasonal (Fig. 12) time scales, the downward phase propagation noted by A14 is seen prominently in several years at all four locations.

The upward propagation of phase leads to a strong coherence between the ADCP current at 48 m and the OSCAR current (Fig. 5) or the ADCP current at 24 m (Fig. 6). This coherence between the ADCP currents at 48 m and 24 m was hinted at by A14, but they had access to only ~ 7 months of data above ~ 40 m. The replacement of the 76 kHz ADCP by a 153 kHz ADCP at the top of the mooring line in 2012 (Tables 1–4) has allowed a more robust analysis of this coherence in depth. As expected from the strong upward phase propagation, the current at 48 m leads that at 24 m, but the downward phase propagation seen at intra-annual and intraseasonal time scales (Figs. 4,9,12) results in the 24 m current leading in these period bands on several occasions.

The alongshore wavelet coherence between Kollam and Mumbai is high at the annual and intra-annual time scales, and Kollam leads Mumbai (Fig. 10). Though the coherence between Goa and Mumbai or Kollam and Goa shows a similar behaviour, the data gaps preclude statistical confidence in the results. At intraseasonal time scales, the coherence is high for adjacent locations on several occasions, but the Kollam–Mumbai coherence does not necessarily reflect what is seen in the Kollam–Goa and Goa–Mumbai coherence.

Use of a 500-day low-pass Lanczos filter reveals strong sub-annual flow off Mumbai and Kollam (Fig. 13). Off Kollam, the sub-annual WICC is mostly poleward and is stronger than the annual WICC (Fig. 9). The sub-annual (Fig. 14) and intra-annual (Fig. 11) currents are associated with eddy-like circulations in the SEAS and the cross-shore component is therefore comparable to or stronger than the alongshore component on some occasions. Off Mumbai, however, the cross-shore flow is weaker than the alongshore flow.

The band-pass filters show that the intraseasonal component of the WICC (Fig. 12) is stronger than the seasonal component (Fig. 9). Therefore, we test the degree of seasonality of the WICC by asking the following question: Does the WICC have a canonical direction for a given season? In other words, is it possible to predict the direction in which the WICC will flow on a given day of the year? To answer this question, we plot the mean of the alongshore WICC for a given day along with the magnitude of the current for that day in each of the years for which data are available. There is considerable scatter about the daily mean off both Mumbai and Kollam for the sub-inertial WICC and it is evident that the WICC on a given day of the year can flow in either direction, poleward or equatorward (Fig. 15). Since the intraseasonal band lies between ~ 30 – 90 days, the 45-day low-passed current is expected to exhibit much lower intraseasonal variability, allowing the seasonality to manifest more clearly. The envelope of one

standard deviation, represented by black curves in Fig. 15, is wider off Kollam than off Mumbai. The zero line almost passes between the black curves over the entire year even for the 45-day low-passed current. Off Mumbai (Kollam), the zero line lies on one side of the curves only for part of November, January, and June (October, November, and September). That it is almost possible to draw a line between the curves representing one standard deviation shows the dominance of intraseasonal variability in the regime of the WICC. Using a 100-day low-pass filter eliminates the intraseasonal variability and the mean therefore represents the climatological seasonal cycle of the WICC and the $1\text{-}\sigma$ curves provide a measure of its interannual variability. The climatological WICC off Mumbai shows the canonical equatorward (poleward) flow during the summer (winter) monsoon. Off Kollam, however, the strong sub-annual poleward flow (Fig. 13) implies that the seasonal WICC is usually poleward, with the magnitude of the poleward current reaching $\sim 15 \text{ cm s}^{-1}$; equatorward flow is much weaker and is restricted to May–July.

This behaviour of the WICC, which can flow in either direction, poleward or equatorward, on any given day of the year, is in contrast to that of the EICC, for which the seasonal cycle dominates and it is possible to guess the direction of flow depending on the season (Soumya Mukhopadhyay, personal communication, 2019). This implication of the dominance of intraseasonal variability in the regime of the WICC is not apparent in the satellite-derived current data and has been made possible only by the long-term measurements made using the ADCP moorings. The ADCP measurements are continuing and three new moorings have been added to the network to decrease the inter-mooring spacing. One mooring each has been deployed between Goa and Kollam (off Udupi) and Goa and Mumbai (off Jaigarh) and another off Okha to the north of the Mumbai mooring on the continental slope (Fig. 1). This expansion of the network and the standardisation of the mooring layout will allow a more complete time series to be established over the top $\sim 400 \text{ m}$ of the water column in the regime of the WICC. The use of the 153 kHz ADCP has enabled sampling up to $\sim 20 \text{ m}$ from the surface, which is useful in view of the shallow mixed layers that often prevail in the SEAS (Shetye et al., 1990, 1991b; Chatterjee et al., 2012).

As noted in A14, Mukherjee et al. (2018), and Mukherjee and Kalita (2019), the data from these ADCP moorings present a challenge to the numerical models, just as did the hydrographic data from the cruises of the 1980s and 1990s (Shetye et al., 1990, 1991b,a, 1993, 1996; Shetye and Gouveia, 1998). Comparison of the alongshore current simulated by ECCO2 at 45 m with the ADCP current at 48 m (Fig. 16) shows a low correlation, ranging from 0.28 off Kanyakumari to 0.39 off Goa. The HyCOM reanalysis current at 50 m shows a better correlation off Kollam (0.69) and Kanyakumari (0.65), but the correlation decreases to 0.55 off Mumbai and Goa. A wavelet analysis shows (figure not shown) that the lower correlation off these two northern locations is due to a poor simulation of the intraseasonal variability, suggesting significant alongshore variation in the ability of even a sophisticated model reanalysis in simulating the observed WICC. Finally, even for HyCOM, the correlation decreases sharply below $\sim 200 \text{ m}$. Therefore, the state-of-the-art models are successful in simulating the observed seasonal cycle of the WICC, but simulating the intraseasonal variability remains a challenge.

Acknowledgements

The ADCP mooring project has been supported by grants from the Council of Scientific and Industrial Research (CSIR) (under the Supra-Institutional Program of CSIR-NIO during 2007–2012, under OCEAN FINDER during 2012–2017, and TRIMFish thereafter) and the Ministry of Earth Sciences (MoES, via INCOIS) through its programme on Ocean Observing Networks. The support from INCOIS, the CSIR-NIO ship cell, and the officers and crew on board the research vessels are acknowledged with gratitude.

A. Chaudhuri was supported by the Science and Engineering Research Board (SERB) vide project PDF/2017/000302. Ferret has been used for analysis and Ferret and GMT (Generic Mapping Tools) have been used for graphics; the FORTRAN code for wavelet analysis and the *R* package for wavelet coherence spectra were downloaded from <http://paos.colorado.edu/research/wavelets> and <http://tocsy.agnld.uni-potsdam.de/wavelets>, respectively. The OSCAR data were obtained from the Physical Oceanography DAAC of the JetPropulsion Laboratory (downloaded from <http://www.oscar.noaa.gov/>). The SSHA altimeter product was produced and distributed by the Copernicus Marine and Environment Monitoring Service (CMEMS) (<http://www.marine.copernicus.eu>) The ECCO2 Ocean State estimate was downloaded from ftp://ecco.jpl.nasa.gov/ECCO2/cube92_latlon_quart_90S90N/ and the HyCOM Reanalysis product from <https://hycom.org/dataserver/gofs-3pt1/reanalysis>. The validation of these two model-based data products is due to the comments received from an anonymous reviewer. This is CSIR-NIO contribution xxxx.

References

- Amol, P., Shankar, D., Aparna, S. G., Shenoi, S. S. C., Fernando, V., Shetye, S. R., Mukherjee, A., Agarvadekar, Y., Khalap, S. T., Satelkar, N. P., 2012. Observational evidence from direct current measurements for propagation of remotely forced waves on the shelf off the west coast of India. *J. Geophys. Res.* 117, doi:10.1029/2011JC007606.
- Amol, P., Shankar, D., Fernando, V., Mukherjee, A., Aparna, S. G., Fernandes, R., Michael, G. S., Khalap, S. T., Satelkar, N. P., Agarvadekar, Y., Gaonkar, M. G., Tari, A. P., Kankonkar, A., Vernekar, S. P., 2014. Observed intraseasonal and seasonal variability of the West India Coastal Current on the continental slope. *J. Earth Syst. Sci.* 123, 1045–1074, doi:10.1007/s12040-014-0449-5.
- AVISO, 1996. AVISO User Handbook: Merged TOPEX/Poseidon Products. Tech. rep., Collecte Localisation Satellites, France.
- Bell, C., Vassie, J. M., Woodworth, P. L., 1998. POL/PSMSL Tidal Analysis Software Kit 2000 TASK-2000). Tech. rep., Permanent Service for Mean Sea Level, UK.
- Bonjean, F., Lagerloef, G. S. E., 2002. Diagnostic model and analysis of the surface currents in the tropical Pacific Ocean. *J. Phys. Oceanogr.* 32, 2938–2954, doi:10.1175/1520-0485(2002)032<2938:DMAAOT>2.0.CO;2.
- Chassignet, E. P., Hurlburt, H. E., Smedstad, O. M., Halliwell, G. R., Hogan, P. J., Wallcraft, A. J., Baraille, R., Bleck, R., 2007. The hycom (hybrid coordinate ocean model) data assimilative system. *Journal of Marine Systems* 65 (1-4), 60–83.
- Chatterjee, A., Shankar, D., Shenoi, S. S. C., Reddy, G. V., Michael, G. S., Ravichandran, M., Gopalkrishna, V. V., Rao, E. P. R., Bhaskar, T. V. S. U., Sanjeevan, V. N., 2012. A new atlas of temperature and salinity for the north Indian Ocean. *J. Earth Syst. Sci.* 121, 559–593, doi:10.1007/s12040-012-0191-9.
- Duchon, C. E., 1979. Lanczos filtering in one and two dimensions. *J. Appl. Meteorol.* 18, 1016–1022.
- Johannessen, O. M., Subbaraju, G., Blindheim, J., 1987. Seasonal variations of the oceanographic conditions off the southwest coast of India during 1971–1975. *FiskDir. Skr. Ser. HavUnders* 18, 247–261.
- Kutsuwada, K., McPhaden, M., 2002. Intraseasonal variations in the upper equatorial Pacific Ocean prior to and during the 1997–98 El Niño. *J. Phys. Oceanogr.* 32 (4), 1133–1149, doi:10.1175/1520-0485(2002)032<1133:IVITUE>2.0.CO;2.
- Maraun, D., Kurths, J., 2004. Cross wavelet analysis. significance testing and pitfalls. *Nonlinear Process. Geophys.* 11, 505–514.
- Maraun, D., Kurths, J., Holschneider, M., 2007. Nonstationary gaussian processes in wavelet domain: Synthesis, estimation and significance testing. *Phys. Rev. E* 75, 016707.
- McCreary, J. P., Kundu, P. K., Molinari, R. L., 1993. A numerical investigation of dynamics, thermodynamics and mixed-layer processes in the Indian Ocean. *Prog. Oceanogr.* 31, 181–244, doi:10.1016/0079-6611(93)90002-U.
- Menemenlis, D., Campin, J.-M., Heimbach, P., Hill, C., Lee, T., Nguyen, A., Schodlok, M., Zhang, H., 2008. Ecco2: High resolution global ocean and sea ice data synthesis. *Mercator Ocean Quarterly Newsletter* 31 (October), 13–21.

- Mukherjee, A., Kalita, B., 2019. Signature of La Niña in interannual variations of the East India Coastal Current during spring. *Clim. Dyn.* 52, 1–18, doi:10.1007/s00382-018-4601-9.
- Mukherjee, A., Shankar, D., Chatterjee, A., Vinayachandran, P. N., 2018. Numerical simulation of the observed near-surface East India Coastal Current on the continental slope. *Clim. Dyn.* 50, 3949–3980, doi:10.1007/s00382-017-3856-x.
- Mukherjee, A., Shankar, D., Fernando, V., Amol, P., Aparna, S. G., Fernandes, R., Michael, G. S., Khalap, S. T., Satelkar, N. P., Agarvadekar, Y., Gaonkar, M. G., Tari, A. P., Kankonkar, A., Vernekar, S. P., 2014. Observed seasonal and intraseasonal variability of the East India Coastal Current on the continental slope. *J. Earth Syst. Sci.* 123, 1197–1232, doi:10.1007/s12040-014-0471-7.
- Mukhopadhyay, S., Shankar, D., Aparna, S. G., Mukherjee, A., 2017. Observations of the sub-inertial, near-surface east india coastal current. *Cont. Shelf. Res.* 148, 159–177, doi:10.1016/j.csr.2017.08.020.
- Schott, F. A., McCreary, J. P., 2001. The monsoon circulation of the Indian Ocean. *Prog. Oceanogr.* 51, 1–123, dOI:10.1016/S0079-6611(01)00083-0.
- Shankar, D., 2000. Seasonal cycle of sea level and currents along the coast of India. *Curr. Sci.* 78, 279–288.
- Shankar, D., Shetye, S. R., 1997. On the dynamics of the Lakshadweep high and low in southeastern Arabian Sea. *J. Geophys. Res.* 102, 12551–12562.
- Shankar, D., Vinayachandran, P. N., Unnikrishnan, A. S., 2002. The monsoon currents in the north Indian Ocean. *Prog. Oceanogr.* 52, 63–120, doi:10.1016/S0079-6611(02)00024-1.
- Shetye, S., Shenoi, S., Gouveia, A., Michael, G., Sundar, D., Nampoothiri, G., 1991a. Wind-driven coastal upwelling along the western boundary of the Bay of Bengal during the southwest monsoon. *Cont. Shelf. Res.* 11, 1397–1408, doi:10.1016/0278-4343(91)90042-5.
- Shetye, S. R., 1998. West India Coastal Current and Lakshadweep high/low. *Sadhana* 23, 637–651.
- Shetye, S. R., Gouveia, A. D., 1998. Coastal circulation in the north Indian Ocean: Coastal segment (14, SW). In: Robinson, A. R. (Ed.), *The Sea*. John Wiley and Sons, New York, USA, pp. 523–556.
- Shetye, S. R., Gouveia, A. D., Shankar, D., Shenoi, S. S. C., Vinayachandran, P. N., Sundar, D., Michael, G. S., Nampoothiri, G., 1996. Hydrography and circulation in the western Bay of Bengal during the northeast monsoon. *J. Geophys. Res.* 101, 14011–14025, doi:10.1029/95JC03307.
- Shetye, S. R., Gouveia, A. D., Shenoi, S. S. C., Michael, G. S., Sundar, D., Almeida, A. M., Santanam, K., 1991b. The coastal current off western India during the northeast monsoon. *Deep Sea Res.* 38, 1517–1529.
- Shetye, S. R., Gouveia, A. D., Shenoi, S. S. C., Sundar, D., Michael, G. S., Almeida, A. M., Santanam, K., 1990. Hydrography and circulation off the west coast of India during the southwest monsoon 1987. *J. Mar. Res.* 48, 359–378.
- Shetye, S. R., Gouveia, A. D., Shenoi, S. S. C., Sundar, D., Michael, G. S., Nampoothiri, G., 1993. The western boundary current of the seasonal subtropical gyre in the Bay of Bengal. *J. Geophys. Res.* 98, 945–954, doi:10.1029/92JC02070.
- Shetye, S. R., Shenoi, S. S. C., 1988. Seasonal cycle of surface circulation in the coastal North Indian Ocean. *Proc. Indian Acad. Sci. (Earth Planet Sci.)* 97 (1), 53–62.

- Sikhakolli, R., Sharma, R., Basu, S., Gohil, B. S., Sarkar, A., Prasad, K. V. S. R., 2013. Evaluation of OSCAR ocean surface current product in the tropical Indian Ocean using in-situ data. *J. Earth Syst. Sci.* 122, 187–199.
- Torrence, C., Compo, G. P., 1998. A practical guide to wavelet analysis. *Bull. Am. Meteorol. Soc.* 79 (1), 61–78, doi:10.1175/1520-0477(1998)079<3C0061:APGTWA>3E2.0.CO;2.
- Vialard, J., Shenoi, S. S. C., McCreary, J. P., Shankar, D., Durand, F., Fernando, V., Shetye, S. R., 2009. Intraseasonal response of the northern Indian Ocean coastal waveguide to the Madden-Julian oscillation. *Geophys. Res. Lett.* 36, doi:10.1029/2009GL038450.

ADCP	Position / Depth	Start date	End date	ADCP depth	ν
M1	69.232 19.996 / 1118	21/10/08	02/11/09	361	76.8
M2	69.236 19.999 / 1096	02/11/09	06/11/10	341	76.8
M3	69.233 19.998 / 1128	06/11/10	16/10/11	355	76.8
M4	69.233 19.999 / 1133	16/10/11	05/10/12	350	76.8
M5A	69.233 20.000 / 1134	05/10/12	16/11/13	160	153.6
M5B		05/10/12	16/11/13	339	153.6
M5C		05/10/12	27/07/13	849	76.8
M6A	69.232 20.000 / 1155	16/11/13	02/11/14	182	153.6
M6B		16/11/13	02/11/14	358	153.6
M7A	69.241 20.013 / 1122	02/11/14	02/01/16	172	153.6
M7B		02/11/14	02/01/16	350	76.8
M8A	69.239 20.012 / 1140	02/01/16	09/11/16	194	153.6
M8B		02/01/16	09/11/16	371	76.8
M9A	69.238 20.011/ 1118	09/11/16	09/11/17	160	153.6
M9B		09/11/16	09/11/17	285	153.6
M9C		09/11/16	09/11/17	647	76.8
M10A	69.238 20.011 / 1073	09/11/17	29/09/18	148	153.6
M10B		09/11/17	29/09/18	271	153.6

Table 1: Details of the ADCP mooring data off **Mumbai**. The columns are as follows. C1: the name of the ADCP, with A, B, and C denoting the first, second, and third ADCPs from top to bottom for years in which there were multiple ADCPs along the mooring line. C2: Longitude ($^{\circ}$ E) and latitude ($^{\circ}$ N) of the mooring location and the water column depth (m). C3 and C4 : Start date and end date, respectively of the record for the deployment. C5: ADCP depth (m). C6: ADCP frequency (kHz). The data gaps are scattered and are shown in Fig. 3. The measurements are available hourly at a depth resolution of 8 m (4 m) for the 76 kHz (153 kHz) ADCPs. All ADCPs off Mumbai are upward-looking and the coastline angle is 7° , measured anticlockwise from the north (Amol et al., 2014).

ADCP	Position / Depth	Start date	End date	ADCP depth	ν
G4	72.714 15.155 / 1130	17/10/08	04/11/09	336	76.8
G5	72.714 15.155 / 1085	04/11/09	05/11/10	348	76.8
G6	72.714 15.155 / 1115	05/11/10	14/10/11	344	76.8
G7A	72.714 15.155 / 970	27/10/11	15/12/11	124	153.6
G7B (D)		27/10/11	15/12/11	175	307.3
G7C		27/10/11	15/12/11	862	76.8
G7A1	72.749 15.164 / 944	15/12/11	23/06/12	174	153.6
G7B1 (D)		15/12/11	15/04/12	225	307.3
G7C1		15/12/11	30/07/12	912	76.8
G8A	72.751 15.165 / 952	09/10/12	08/11/13	161	153.6
G8B		09/10/12	09/11/13	346	153.6
G8C		09/10/12	04/07/13	850	76.8
G9A	72.757 15.164 / 960	11/11/13	21/04/14	163	153.6
G9B		11/11/13	19/10/14	339	153.6
G10A	72.745 15.165 / 979	20/10/14	06/01/16	190	153.6
G10B		20/10/14	06/01/16	410	76.8
G11A	72.744 15.165 / 976	06/01/16	12/11/16	177	153.6
G11B		06/01/16	12/11/16	388	76.8
G12A	72.744 15.166 / 984	12/11/16	03/10/17	161	153.6
G12B		12/11/16	03/10/17	287	153.6
G12C		12/11/16	03/10/17	652	76.8
G13A	72.744 15.166 / 996	03/10/17	25/09/18	171	153.6
G13B		03/10/17	25/09/18	296	153.6
G13C		03/10/17	25/09/18	661	76.8

Table 2: Details of the ADCP mooring data off **Goa**. The columns are as follows. C1: the name of the ADCP, with A, B, and C denoting the first, second, and third ADCPs from top to bottom for years in which there were multiple ADCPs along the mooring line. C2: Longitude ($^{\circ}$ E) and latitude ($^{\circ}$ N) of the mooring location and the water column depth (m). C3 and C4 : Start date and end date, respectively of the record for the deployment. C5: ADCP depth (m). C6: ADCP frequency (kHz). The data gaps are scattered and are shown in Fig. 3. The measurements are available hourly at a depth resolution of 8 m (4 m) for the 76 kHz (153 kHz) ADCPs. Downward-looking ADCPs are indicated by “(D)” in C1 and the coastline angle is 14° , measured anticlockwise from the north (Amol et al., 2014).

ADCP	Position / Depth	Start date	End date	ADCP depth	ν
K2	75.436 9.050 / 1195	29/10/09	12/11/10	348	76.8
K3	75.438 9.045 / 1130	12/11/10	22/10/11	360	76.8
K4	75.438 9.046 / 1133	22/10/11	12/10/12	417	76.8
K5A	75.272 9.046 / 1105	12/10/12	05/11/13	196	153.6
K5B		12/10/12	22/11/13	377	153.6
K6A	75.438 9.046 / 1102	22/11/13	24/10/14	152	153.6
K6B		22/11/13	24/10/14	633	76.8
K7A	75.436 9.051 / 1164	24/10/14	09/01/16	204	153.6
K7B		24/10/14	09/01/16	386	153.6
K8A	75.436 9.048 / 1122	09/01/16	15/11/16	167	153.6
K8B		09/01/16	15/11/16	344	153.6
K8C		09/01/16	15/11/16	858	76.8
K9A	75.435 9.048 / 1183	15/11/16	06/10/17	228	153.6
K9B		15/11/16	06/10/17	388	153.6
K10A	75.435 9.047 / 1170	07/10/17	08/10/18	197	153.6
K10B		07/10/17	08/10/18	376	153.6

Table 3: Details of the ADCP mooring data off **Kollam**. The columns are as follows. C1: the name of the ADCP, with A, B, and C denoting the first, second, and third ADCPs from top to bottom for years in which there were multiple ADCPs along the mooring line. C2: Longitude ($^{\circ}$ E) and latitude ($^{\circ}$ N) of the mooring location and the water column depth (m). C3 and C4 : Start date and end date, respectively of the record for the deployment. C5: ADCP depth (m). C6: ADCP frequency (kHz). The data gaps are scattered and are shown in Fig. 3. The measurements are available hourly at a depth resolution of 8 m (4 m) for the 76 kHz (153 kHz) ADCPs. All ADCPs off Kollam are upward-looking and the coastline angle is 7° , measured anticlockwise from the north (Amol et al., 2014).

ADCP	Position / Depth	Start date	End date	ADCP depth	ν
KK1	77.400 6.961 / 1030	28/10/09	13/11/10	330	76.8
KK2	77.398 6.962 / 995	16/11/10	24/10/11	321	76.8
KK3A	77.397 6.964 / 995	24/10/11	14/10/12	279	76.8
KK3B (D)		24/10/11	30/05/12	305	307.3
KK4A	77.397 6.962 / 1004	14/10/12	24/11/13	366	76.8
KK5A	77.402 6.964 / 996	24/11/13	15/11/14	422	76.8
KKx	MOORING LOST	15/11/14	12/01/16		
KK6A	77.394 6.962 / 1016	12/01/16	16/11/16	174	153.6
KK6B		12/01/16	16/11/16	354	153.6
KKD7A	77.392 6.959 / 1091	16/11/16	08/10/17	246	153.6
KKD7B		16/11/16	08/10/17	501	76.8
KKD8A	77.392 6.959 / 1050	08/10/17	10/10/18	177	153.6
KKD8B		08/10/17	10/10/18	432	76.8

Table 4: Details of the ADCP mooring data off **Kanyakumari**. The columns are as follows. C1: the name of the ADCP, with A, B, and C denoting the first, second, and third ADCPs from top to bottom for years in which there were multiple ADCPs along the mooring line. C2: Longitude ($^{\circ}$ E) and latitude ($^{\circ}$ N) of the mooring location and the water column depth (m). C3 and C4 : Start date and end date, respectively of the record for the deployment. C5: ADCP depth (m). C6: ADCP frequency (kHz). The data gaps are scattered and are shown in Fig. 3. There is a very long gap off Kanyakumari owing to the loss of the mooring during November 2014 to January 2016. The measurements are available hourly at a depth resolution of 8 m (4 m) for the 76 kHz (153 kHz) ADCPs. Downward-looking ADCPs are indicated by “(D)” in C1 and the coastline angle is 90° , measured anticlockwise from the north (Amol et al., 2014).

Fig. 1

The region of interest, the eastern Arabian Sea, and its location in the larger region, the north Indian Ocean. The colour scale shows the bathymetry (metres). The 1000 m contour is overlaid. The solid yellow circles indicate the ADCP locations on the continental slope off Mumbai, Goa, Kollam, and Kanyakumari. The purple circles show the newer ADCP locations off Jaigarh, Udupi, and Okha.

Fig. 2

The alongshore current (cm s^{-1}) at a depth of 100 m before (black) and subsequent (grey dashed) to making the pressure corrections for the large movement that occurs for KK6A during 30 June to 5 July 2016. This is the largest movement over the record. There are only a few large excursions at Kanyakumari and this is the largest. The time scale over which the movement occurs is very short (~ 1 day), and, therefore, the effect of these movements on the sub-inertial currents is insignificant.

Fig. 3

The sub-inertial alongshore current (cm s^{-1}) at all four mooring locations. A poleward current is positive off Mumbai, Goa, and Kollam, and a westward current is positive off Kanyakumari; this sign convention, in which a downwelling (upwelling) favourable current is positive (negative), is also used in all subsequent figures showing the alongshore currents. The odd panels show the current at 48 m (red), 100 m (green), and 200 m (blue) and the even panels show the depth-time variation of the sub-inertial current, with the same colours used to mark these depths. The pink and grey shading represent the summer monsoon (June–September) and winter monsoon (November–February), respectively, with March–May and October marking the transition between these seasons. The black vertical line (during 2013) in the even panels marks the end of the period for which Amol et al. (2014) presented the data. Note that the colour scale is not uniform in the even panels. In all eight panels, the vertical blue lines are used to separate the years.

Fig. 4

Morlet wavelet power spectrum ($\text{cm}^2 \text{s}^2$) for the alongshore ADCP current at 48 m at all four mooring locations. The ordinate is the period (days) plotted on a \log_2 scale; a \log_2 scale is also used for the wavelet power, for which the colour scale is not uniform. The vertical black lines are used to separate the years. The thick blue curve represents the cone of influence. The horizontal lines show the 1 year or 365 days (annual band), 180 days (semi-annual band), 120 days, 90 days, and 30 days. The semi-annual and 120-day bands constitute the intra-annual variability and the low-frequency (high-frequency) part of the intraseasonal variability is contained in the 30–90-day band (4–30-day band).

Fig. 5 The sub-inertial alongshore current at all four mooring locations estimated from the ADCP (green curves) and OSCAR (red curves) data is plotted in the odd panels; the ADCP current is at 48 m and the OSCAR current represents an average over the top ~ 30 m. The OSCAR grid point nearest to the ADCP mooring location has been used for the comparison. The pink and grey shading represents the summer and winter monsoons, respectively. The even panels show the wavelet coherence between the ADCP and OSCAR current; the ordinate for these panels is the period (days) plotted on a \log_2 scale. The thick blue curve marks the cone of influence and the coherence above the 95% significance level is marked by the green contours. The phase difference is shown by the arrows, which are marked only if the coherence exceeds 0.5. The OSCAR current leads (lags) the ADCP current in anticlockwise (clockwise) direction. The horizontal lines mark 365, 90, and 30 days on the ordinate. In all eight panels, the vertical black dashed lines are used to separate the years.

Fig. 6 The wavelet coherence between the alongshore ADCP current at 25 m and 48 m off Mumbai,

Goa, and Kollam; data are not available off Kanyakumari at 25 m. The ordinate is the period (days) plotted on a \log_2 scale. The thick blue curve marks the cone of influence and the coherence above the 95% significance level is marked by the green contours. The phase difference is shown by the arrows, which are marked only if the coherence exceeds 0.5. The ADCP current at 48 m leads (lags) the current at 25 m in anticlockwise (clockwise) direction. The horizontal lines from top to bottom mark 365, 180, 120, 90, and 30 days on the ordinate. The vertical lines are used to separate the years. The 48 m current weakly leads the 25 m current off Mumbai and Goa at seasonal time scales, but the phase difference is higher off Kollam.

Fig. 7 The sub-inertial cross-shore current (cm s^{-1}) at all four mooring locations estimated. Offshore or upwelling-favourable flow is positive. The odd panels show the current at 48 m (red), 100 m (green), and 200 m (blue) and the even panels show the depth-time variation of the sub-inertial current, with the same colours used to mark these depths. The pink and grey shading represent the summer monsoon (June–September) and winter monsoon (November–February), respectively, with March–May and October marking the transition between these seasons. The black vertical line (during 2013) in the even panels marks the end of the period for which Amol et al. (2014) presented the data. Note that the colour scale is not uniform in the even panels. In all eight panels, the vertical blue lines are used to separate the years.

Fig. 8 Morlet wavelet power spectrum ($\text{cm}^2 \text{s}^2$) for the cross-shore ADCP current at 48 m at all four mooring locations. The ordinate is the period (days) plotted on a \log_2 scale; a \log_2 scale is also used for the wavelet power, for which the colour scale is not uniform. The vertical black lines are used to separate the years. The thick blue curve represents the cone of influence. The horizontal lines show the 1 year or 365 days (annual band), 180 days (semi-annual band), 120 days, 90 days, and 30 days. The semi-annual and 120-day bands constitute the intra-annual variability and the low-frequency (high-frequency) part of the intraseasonal variability is contained in the 30–90-day band (4–30-day band).

Fig. 9 The seasonal cycle of the alongshore current. The odd (even) panels show the annual (intra-annual) cycle, estimated using a 300–400-day (100–250-day) Lanczos filter, as a function of time (abscissa) and depth (m, ordinate). The colour key is not uniform. The pink and grey shading represent the summer monsoon (June–September) and winter monsoon (November–February), respectively, with March–May and October marking the transition between these seasons. The key at the top (bottom) is for the annual (intra-annual) band. In all eight panels, the vertical blue lines are used to separate the years.

Fig. 10 Alongshore wavelet coherence, with smoothing factors (1,0.25) for the scale and time, of the alongshore WICC at 48 m. The vertical black lines are used to separate the years. The thick blue curve represents the cone of influence and the coherence above the 95% significance level is marked by the green contour. The ordinate is the period (days) plotted on a \log_2 scale. The horizontal lines from top to bottom mark 365, 180, 120, 90, and 30 days on the ordinate. The top panel shows the coherence between Mumbai and Goa, the second panel between Goa and Kollam, the third panel between Kollam and Kanyakumari, and the bottom panel between Mumbai and Kollam. The phase difference is shown by the arrows, which are marked only if the coherence exceeds 0.5. The current at the southern location leads (lags) the current at the northern location in anticlockwise (clockwise) direction.

Fig. 11 Intra-annual variability during 2012–2013 in the SEAS. The top panel shows the 100–250-day band-passed surface alongshore (solid curves) and cross-shore (dashed curves) current (cm s^{-1}) at the mooring location off Kollam. The black (red) curves are for the ADCP (OSCAR) data. The bottom panel is the SLA map, centred on 15 March 2013, overlaid with the OSCAR current vectors; both SLA and

OSCAR current are filtered using a 100–250-days Lanczos filter. Note that the cross-shore component is much stronger than the alongshore component in mid-March 2013.

Fig. 12 Intraseasonal (30–90-days band-pass-filtered) variability of the alongshore current (cm s^{-1}) at the four mooring locations. The vertical black dashed lines are used to separate the years. Strong intraseasonal variability is seen throughout the record and the variability in this band is stronger during the winter monsoon.

Fig. 13 The sub-annual alongshore (AC) and cross-shore (CC) currents (in cm s^{-1}) obtained by applying a 500-day low-pass filter off Kollam and Mumbai. The vertical black dashed lines are used to separate the years. The odd panels show the sub-annual WICC as a function of time (abscissa) and depth (ordinate, m) and the even panels show the sub-annual current based on both ADCP (48 m, black) and OSCAR (red) data. The alongshore (cross-shore) component is plotted in the top (bottom) four panels. The sub-annual alongshore WICC is stronger than the annual alongshore WICC off Kollam; the sub-annual WICC is mostly poleward off Kollam. The cross-shore sub-annual current is also strong off Kollam.

Fig. 14 500-day-low-passed AVISO SLA (cm) and OSCAR current (cm s^{-1}) on 28 February 2013.

Fig. 15 In which direction does the alongshore WICC flow on a given day? The first and fourth panels show the alongshore, sub-inertial WICC (cm s^{-1}) at 48 m off Mumbai (first panel) and Kollam (fourth panel). Positive values imply poleward flow. The solid black curve is the mean for the available data during 2009–2018 and each colour represents the current during a particular year. The dashed black curves mark one standard deviation about the mean. The second and fifth panels show the 45-day low-passed (LP) current off Mumbai (second panel) and Kollam (fifth panel); the Lanczos filter was used for filtering and the solid and dashed black curves and the coloured dots are as in the odd panels. Note the significant scatter of the coloured dots about the mean. The standard deviation is high and the zero line almost passes between the dashed curves over the entire year even for the 45-day low-passed current. Off Mumbai (Kollam), the zero line lies on one side of the curves only for part of November, January, and June (October, November, and September). That it is almost possible to draw a line between the curves representing one standard deviation shows the dominance of intraseasonal variability in the regime of the WICC. The third and sixth panels show the 100-day low-passed WICC off Mumbai (third panel) and Kollam (sixth panel); intraseasonal variability, defined in this paper as the variability in the 30–90-day band, is filtered out, leaving only the variability at higher periods. Therefore, the red curves in these panels represent the climatological seasonal cycle estimated from the ADCP data record. The mean seasonal current off Mumbai shows the canonical equatorward (poleward) flow during the summer (winter) monsoon, but the mean seasonal WICC is largely poleward off Kollam owing to the strong sub-annual flow (Fig. 13). The poleward WICC off Kollam reaches a magnitude of $\sim 15 \text{ cm s}^{-1}$ and the equatorward flow, which is restricted to May–July, is much weaker. The $1-\sigma$ curves in these panels represent the interannual variability, which is large at both locations.

Fig. 16 The sub-inertial alongshore current at all four mooring locations estimated from the ADCP data (red curves), the HyCOM reanalysis (blue curves), and ECCO2 (green curves) is shown as a function of time. The currents shown are at $\sim 48 \text{ m}$. The HyCOM and ECCO2 grid points nearest to the ADCP mooring location has been used for the comparison. The correlation coefficients between the HyCOM and ADCP currents and between the ECCO2 and ADCP currents are shown in blue and green, respectively. The pink and grey shading represent the summer monsoon (June–September) and winter monsoon (November–February), respectively, with March–May and October marking the transition between these seasons.

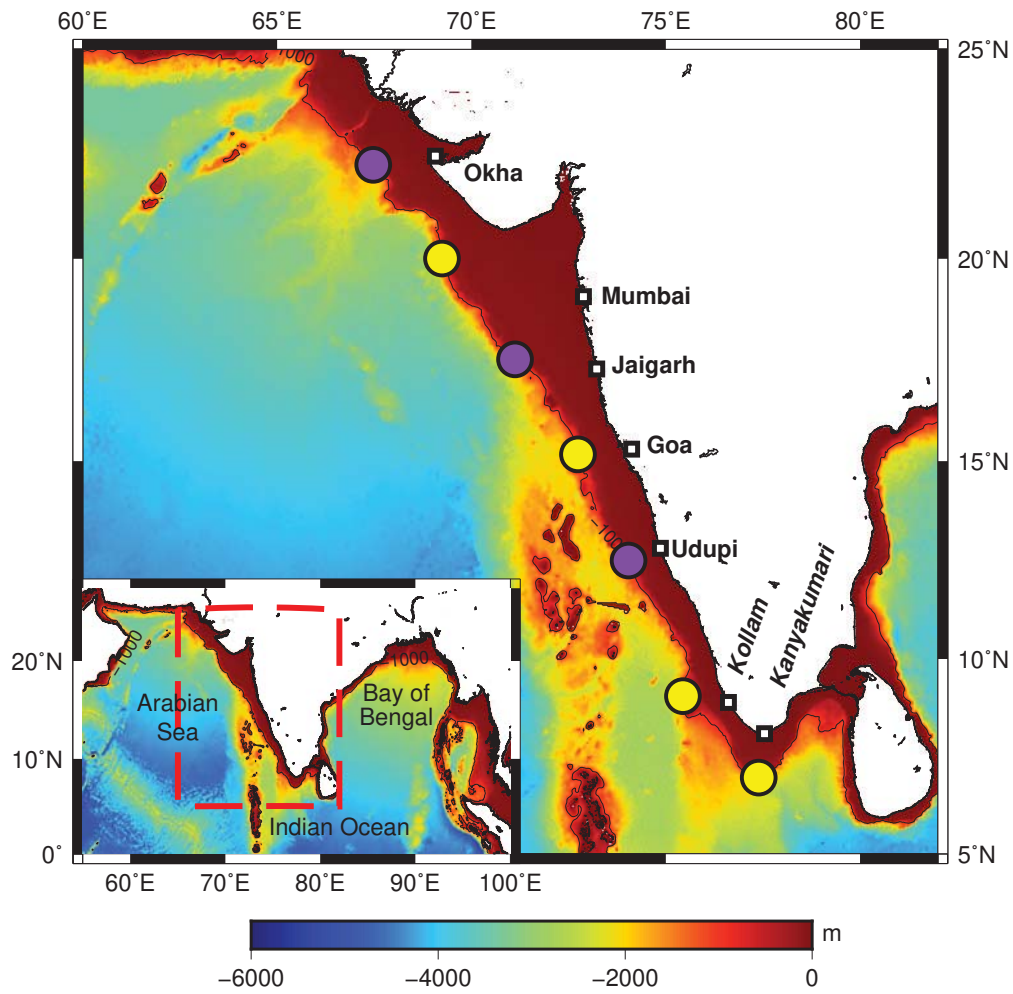


Figure 1: The region of interest, the eastern Arabian Sea, and its location in the larger region, the north Indian Ocean. The colour scale shows the bathymetry (metres). The 1000 m contour is overlaid. The solid yellow circles indicate the ADCP locations on the continental slope off Mumbai, Goa, Kollam, and Kanyakumari. The purple circles show the newer ADCP locations off Jaigarh, Udupi, and Okha.

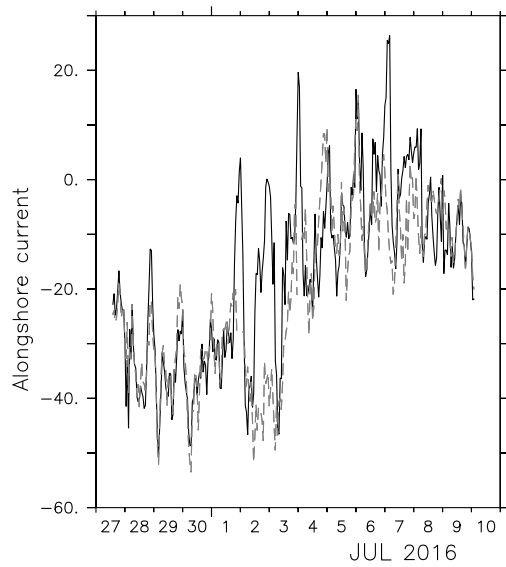


Figure 2: The alongshore current (cm s^{-1}) at a depth of 100 m before (black) and subsequent (grey dashed) to making the pressure corrections for the large movement that occurs for KK6A during 30 June to 5 July 2016. This is the largest movement over the record. There are only a few large excursions at Kanyakumari and this is the largest. The time scale over which the movement occurs is very short (~ 1 day), and, therefore, the effect of these movements on the sub-inertial currents is insignificant.

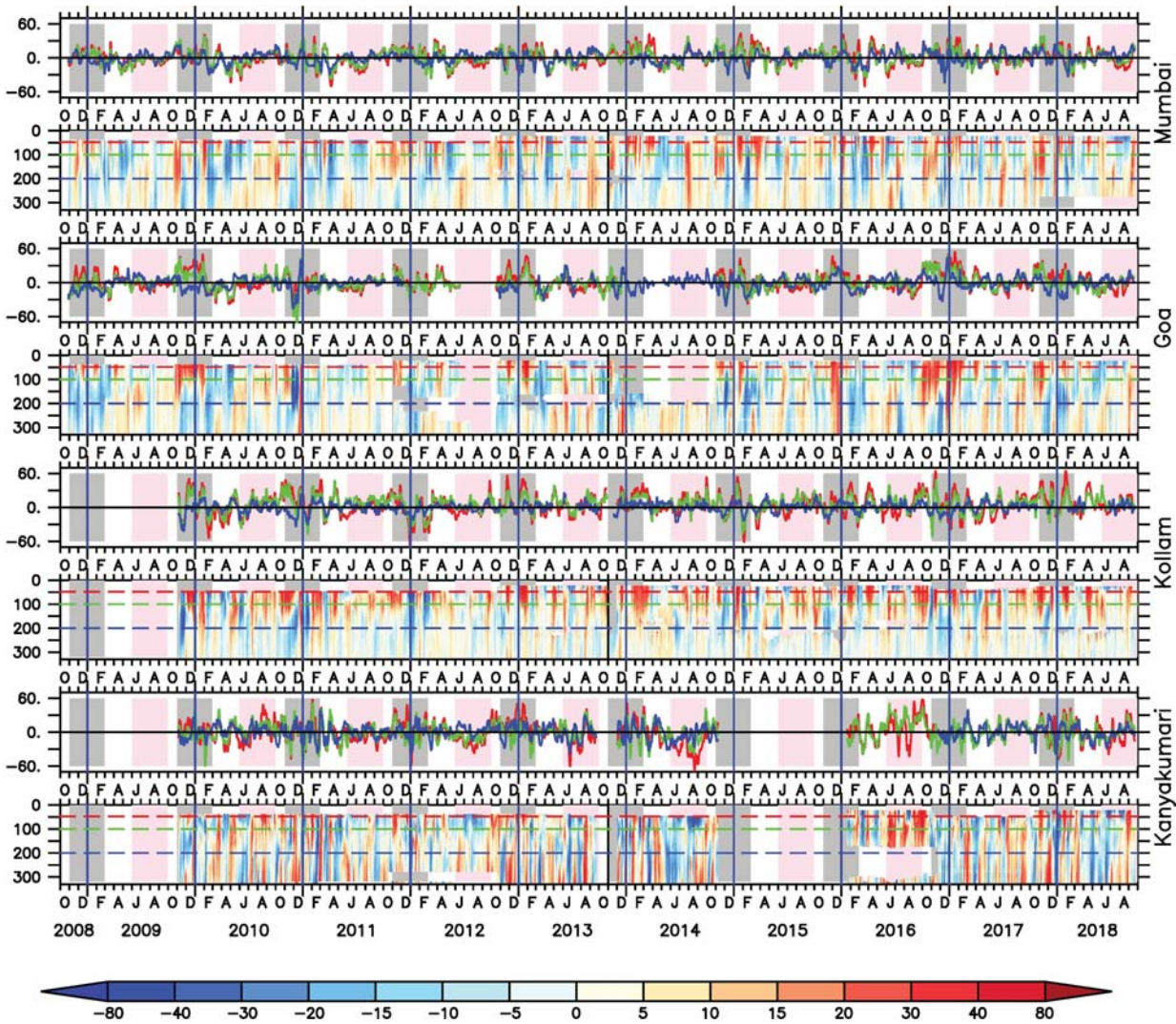


Figure 3: The sub-inertial alongshore current (cm s^{-1}) at all four mooring locations. A poleward current is positive off Mumbai, Goa, and Kollam, and a westward current is positive off Kanyakumari; this sign convention, in which a downwelling (upwelling) favourable current is positive (negative), is also used in all subsequent figures showing the alongshore currents. The odd panels show the current at 48 m (red), 100 m (green), and 200 m (blue) and the even panels show the depth-time variation of the sub-inertial current, with the same colours used to mark these depths. The pink and grey shading represent the summer monsoon (June–September) and winter monsoon (November–February), respectively, with March–May and October marking the transition between these seasons. The black vertical line (during 2013) in the even panels marks the end of the period for which Amol et al. (2014) presented the data. Note that the colour scale is not uniform in the even panels. In all eight panels, the vertical blue lines are used to separate the years.

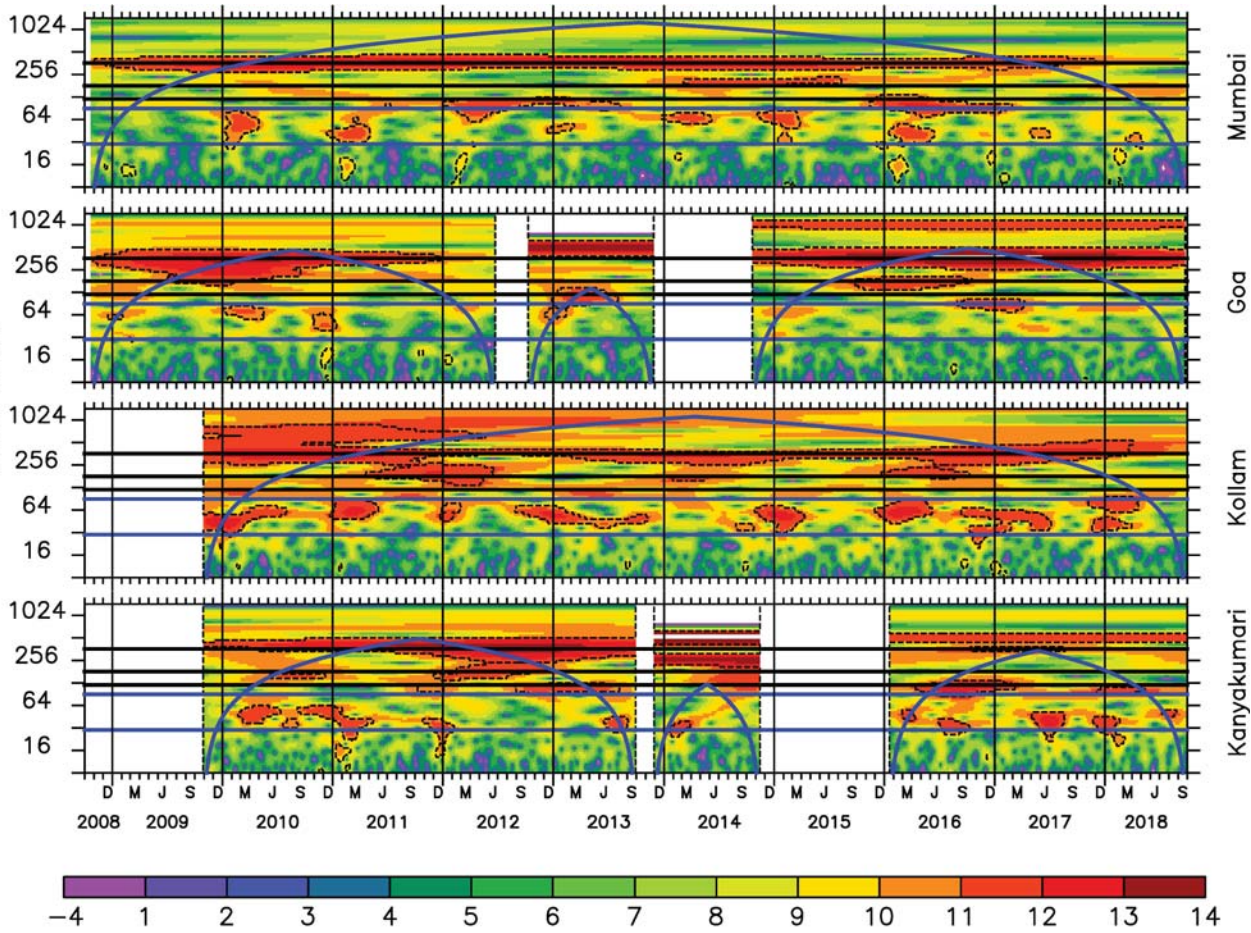


Figure 4: Morlet wavelet power spectrum ($\text{cm}^2 \text{s}^{-2}$) for the alongshore ADCP current at 48 m at all four mooring locations. The ordinate is the period (days) plotted on a \log_2 scale; a \log_2 scale is also used for the wavelet power, for which the colour scale is not uniform. The vertical black lines are used to separate the years. The thick blue curve represents the cone of influence. The horizontal lines show the 1 year or 365 days (annual band), 180 days (semi-annual band), 120 days, 90 days, and 30 days. The semi-annual and 120-day bands constitute the intra-annual variability and the low-frequency (high-frequency) part of the intraseasonal variability is contained in the 30–90-day band (4–30-day band).

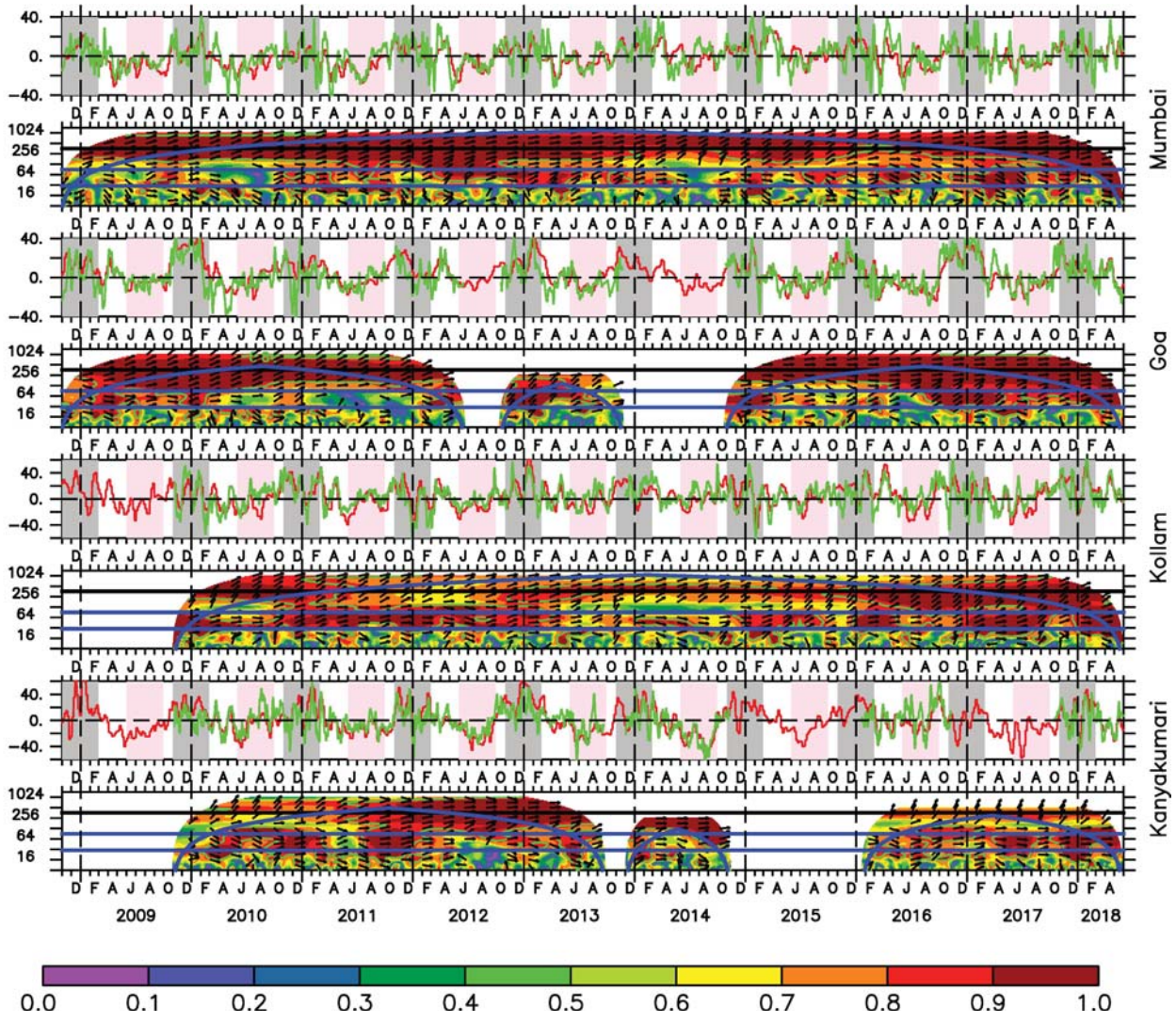


Figure 5: The sub-inertial alongshore current at all four mooring locations estimated from the ADCP (green curves) and OSCAR (red curves) data is plotted in the odd panels; the ADCP current is at 48 m and the OSCAR current represents an average over the top ~30 m. The OSCAR grid point nearest to the ADCP mooring location has been used for the comparison. The pink and grey shading represents the summer and winter monsoons, respectively. The even panels show the wavelet coherence between the ADCP and OSCAR current; the ordinate for these panels is the period (days) plotted on a \log_2 scale. The thick blue curve marks the cone of influence and the coherence above the 95% significance level is marked by the green contours. The phase difference is shown by the arrows, which are marked only if the coherence exceeds 0.5. The OSCAR current leads (lags) the ADCP current in anticlockwise (clockwise) direction. The horizontal lines mark 365, 90, and 30 days on the ordinate. In all eight panels, the vertical black dashed lines are used to separate the years.

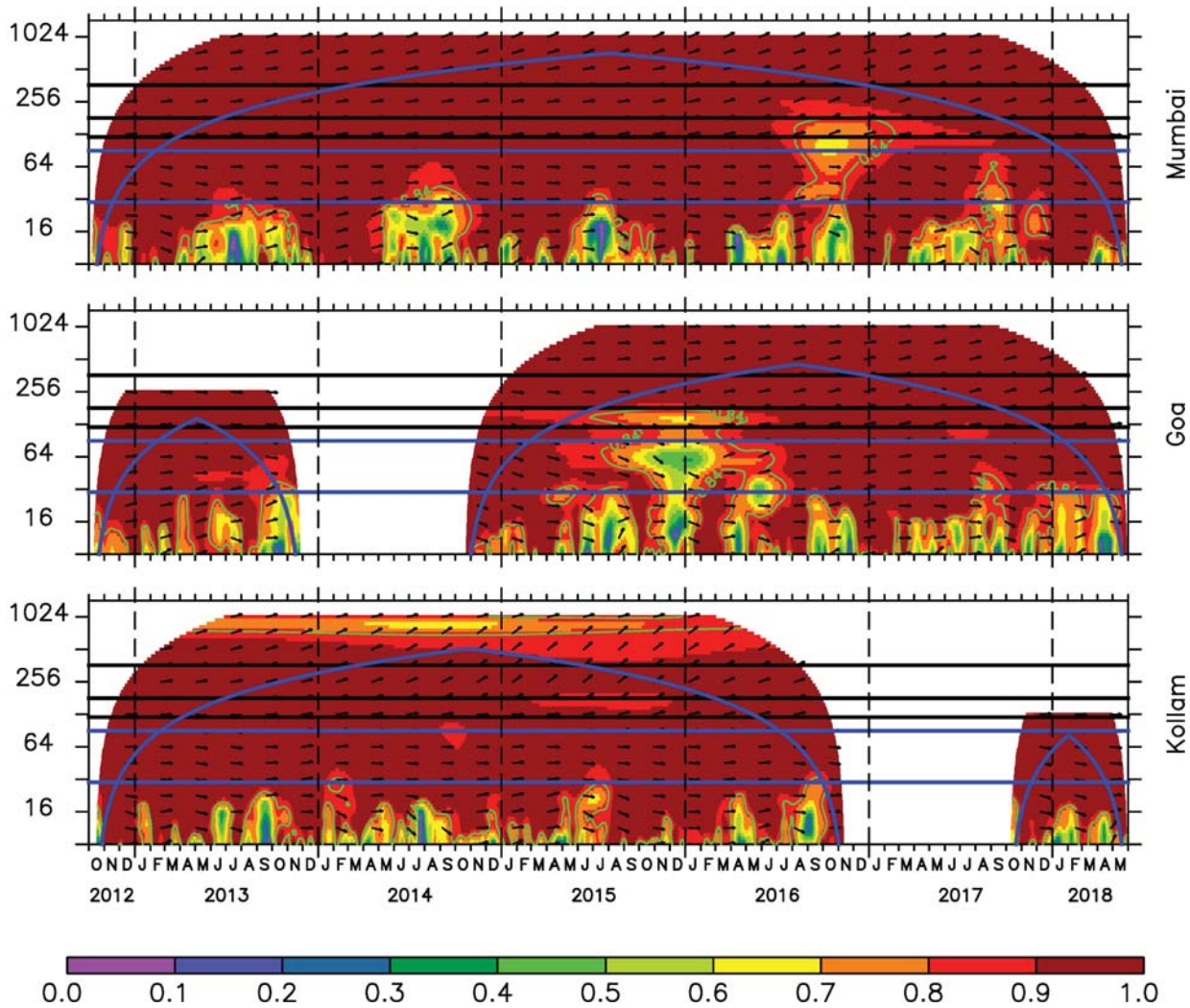


Figure 6: The wavelet coherence between the alongshore ADCP current at 25 m and 48 m off Mumbai, Goa, and Kollam; data are not available off Kanyakumari at 25 m. The ordinate is the period (days) plotted on a \log_2 scale. The thick blue curve marks the cone of influence and the coherence above the 95% significance level is marked by the green contours. The phase difference is shown by the arrows, which are marked only if the coherence exceeds 0.5. The ADCP current at 48 m leads (lags) the current at 25 m in anticlockwise (clockwise) direction. The horizontal lines from top to bottom mark 365, 180, 120, 90, and 30 days on the ordinate. The vertical lines are used to separate the years. The 48 m current weakly leads the 25 m current off Mumbai and Goa at seasonal time scales, but the phase difference is higher off Kollam.

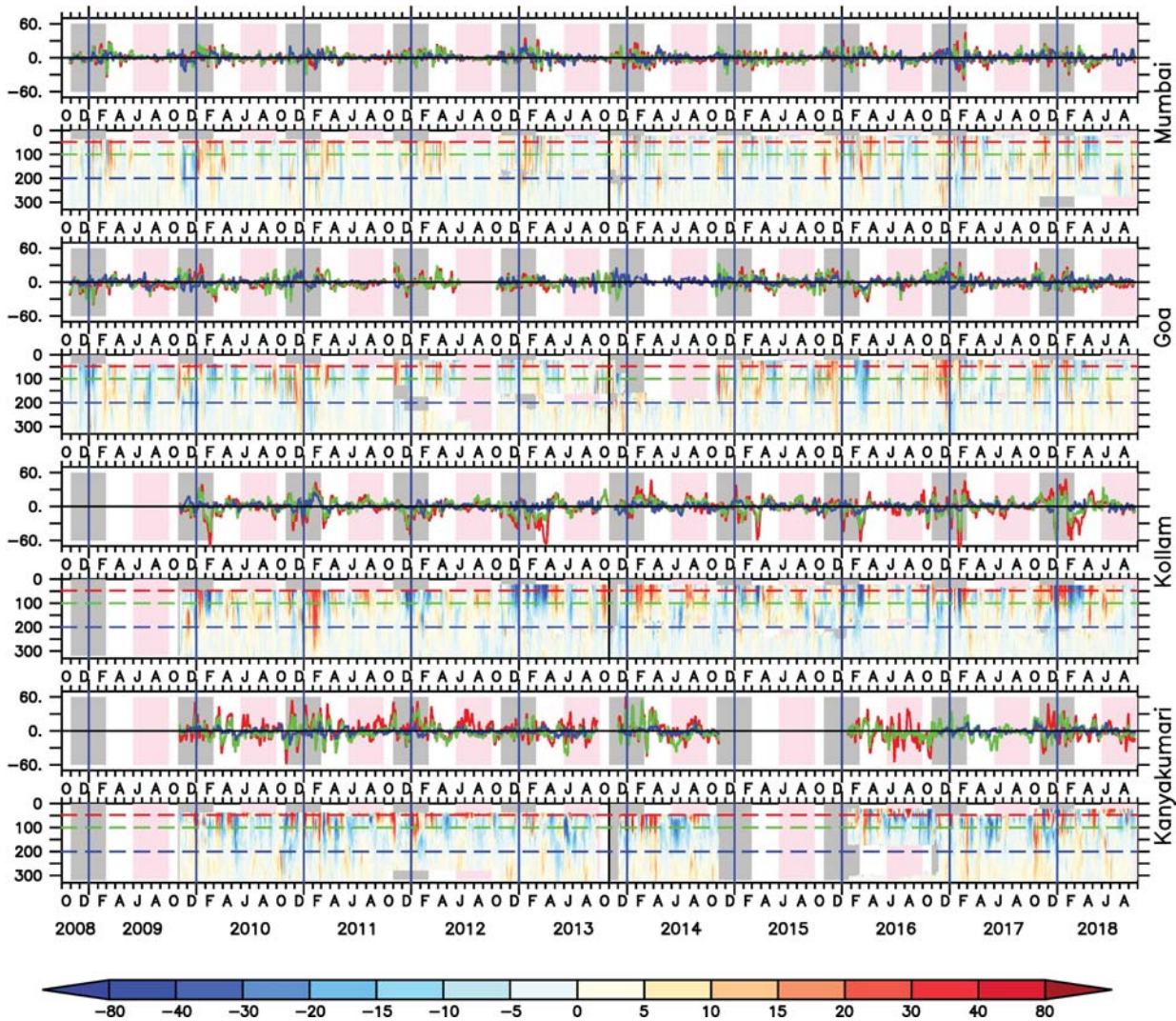


Figure 7: The sub-inertial cross-shore current (cm s^{-1}) at all four mooring locations estimated. Offshore or upwelling-favourable flow is positive. The odd panels show the current at 48 m (red), 100 m (green), and 200 m (blue) and the even panels show the depth-time variation of the sub-inertial current, with the same colours used to mark these depths. The pink and grey shading represent the summer monsoon (June–September) and winter monsoon (November–February), respectively, with March–May and October marking the transition between these seasons. The black vertical line (during 2013) in the even panels marks the end of the period for which Amol et al. (2014) presented the data. Note that the colour scale is not uniform in the even panels. In all eight panels, the vertical blue lines are used to separate the years.

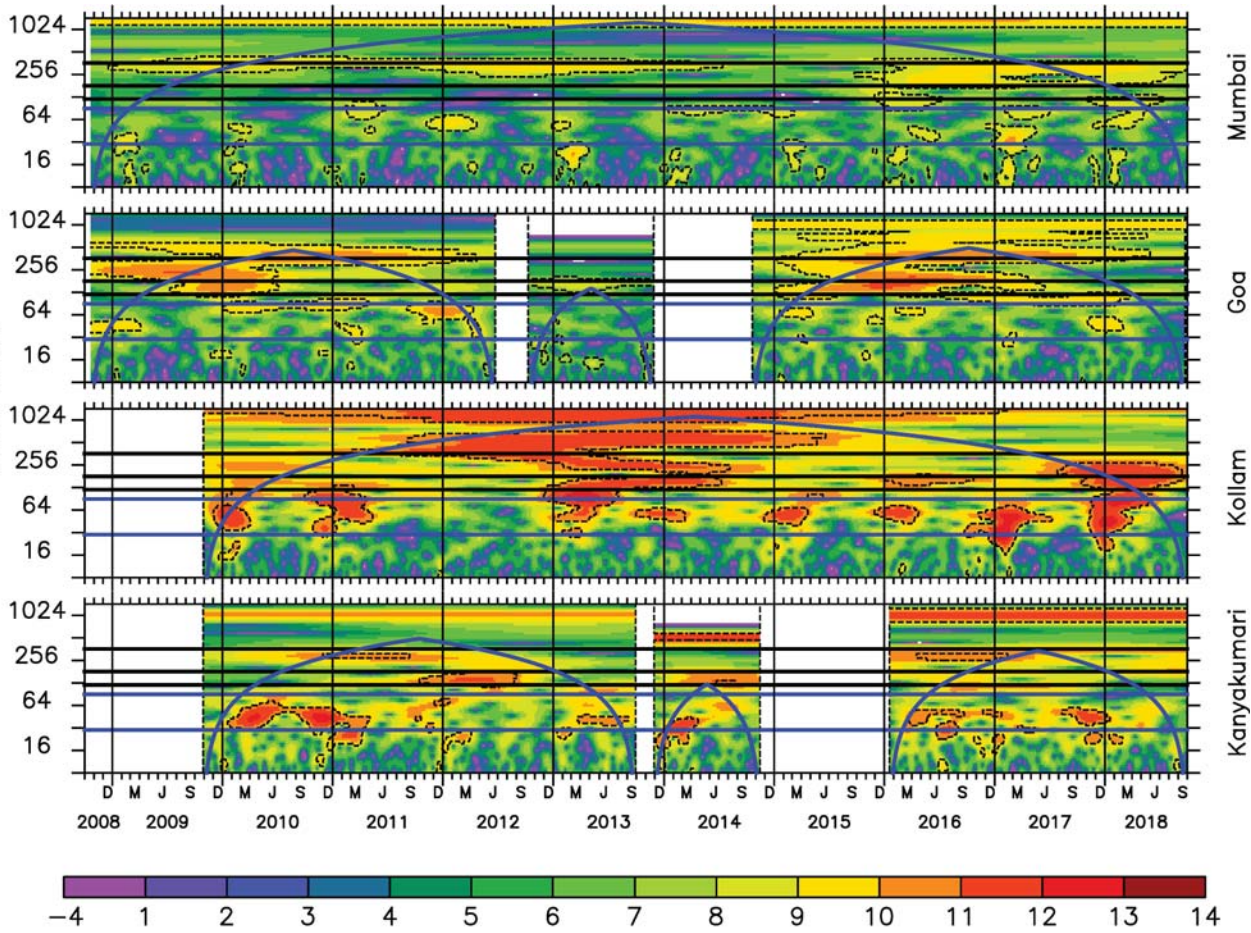


Figure 8: Morlet wavelet power spectrum ($\text{cm}^2 \text{s}^{-2}$) for the cross-shore ADCP current at 48 m at all four mooring locations. The ordinate is the period (days) plotted on a \log_2 scale; a \log_2 scale is also used for the wavelet power, for which the colour scale is not uniform. The vertical black lines are used to separate the years. The thick blue curve represents the cone of influence. The horizontal lines show the 1 year or 365 days (annual band), 180 days (semi-annual band), 120 days, 90 days, and 30 days. The semi-annual and 120-day bands constitute the intra-annual variability and the low-frequency (high-frequency) part of the intraseasonal variability is contained in the 30–90-day band (4–30-day band).

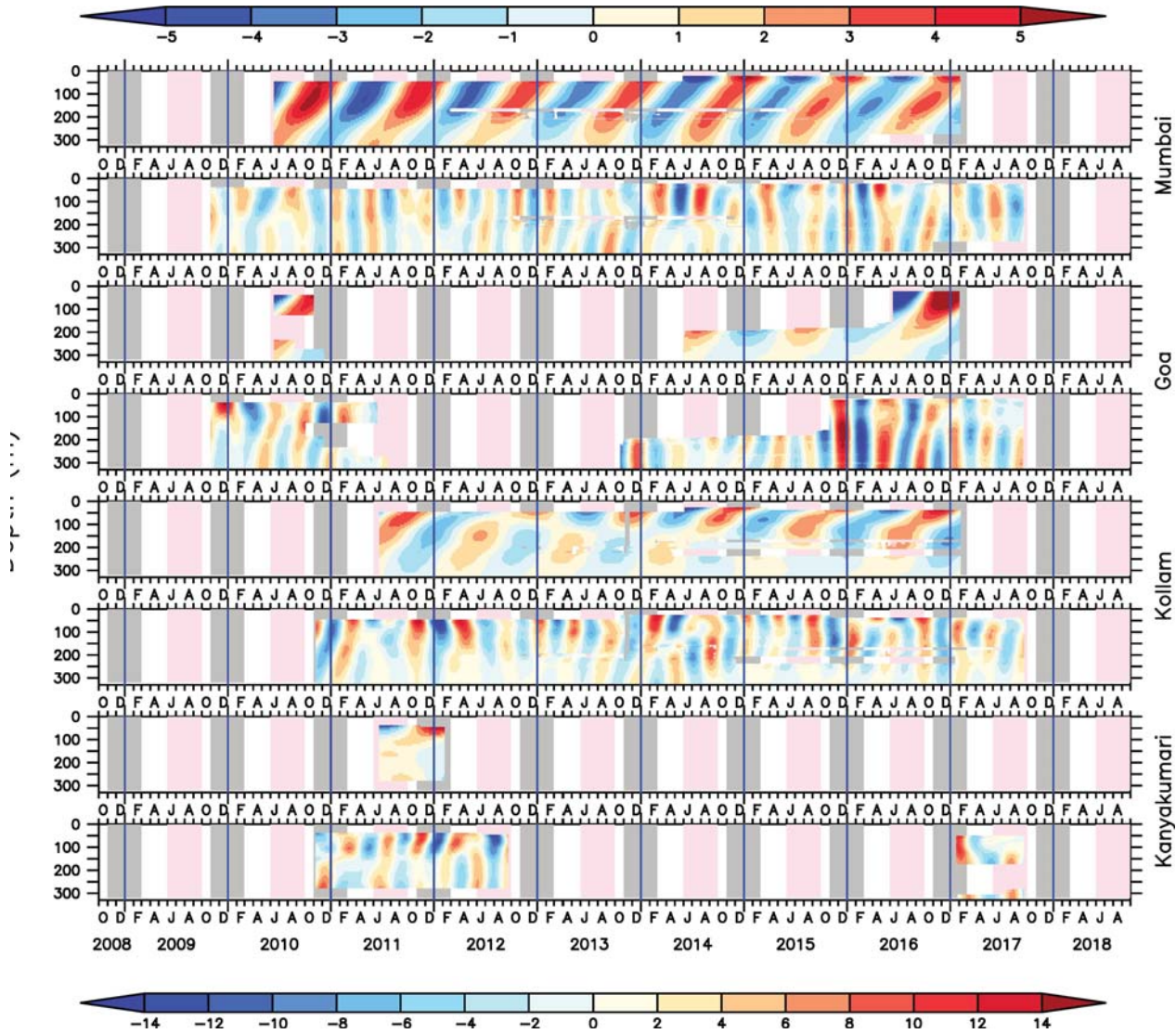


Figure 9: The seasonal cycle of the alongshore current. The odd (even) panels show the annual (intra-annual) cycle, estimated using a 300–400-day (100–250-day) Lanczos filter, as a function of time (abscissa) and depth (m, ordinate). The colour key is not uniform. The pink and grey shading represent the summer monsoon (June–September) and winter monsoon (November–February), respectively, with March–May and October marking the transition between these seasons. The key at the top (bottom) is for the annual (intra-annual) band. In all eight panels, the vertical blue lines are used to separate the years.

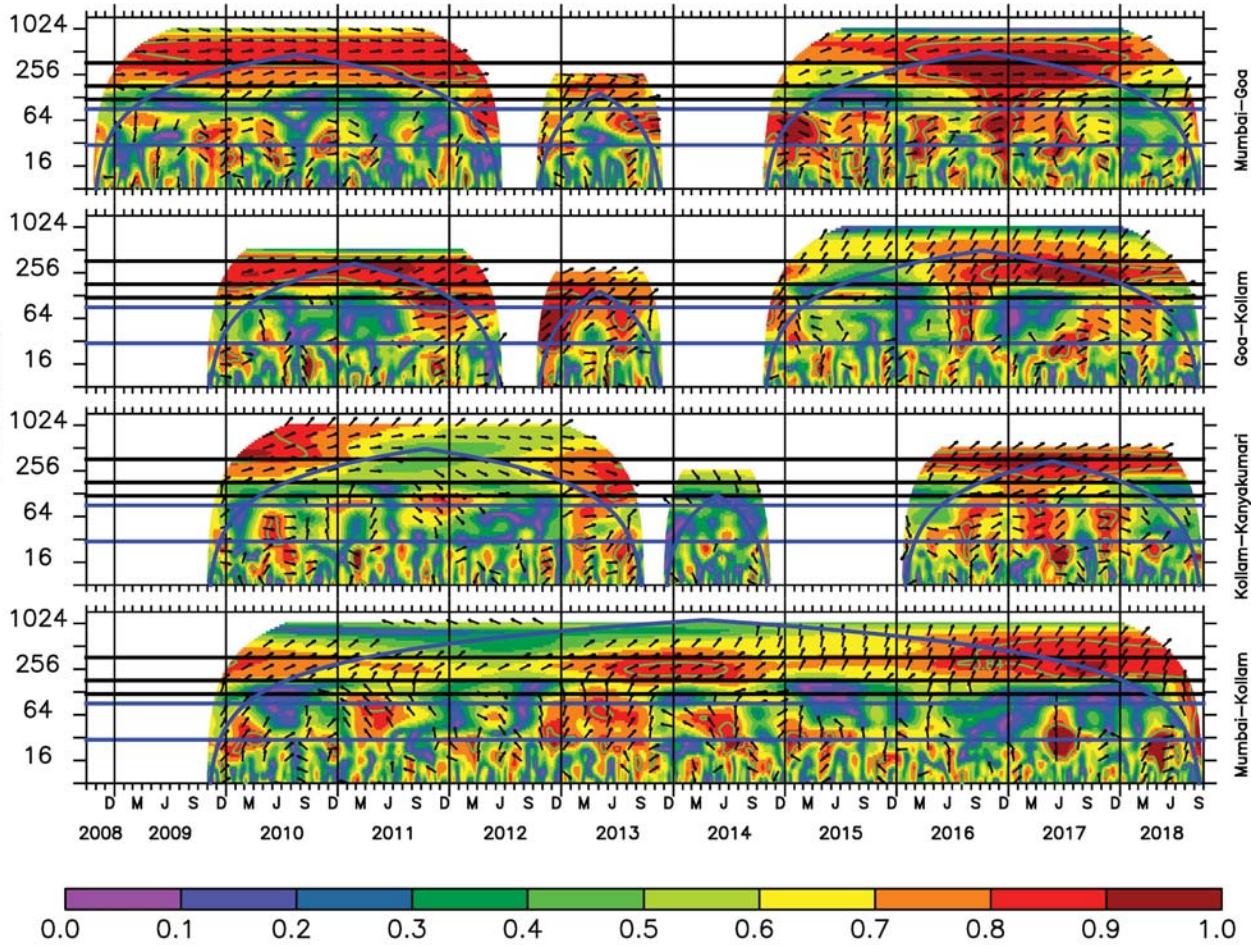


Figure 10: Alongshore wavelet coherence, with smoothing factors (1,0.25) for the scale and time, of the alongshore WICC at 48 m. The vertical black lines are used to separate the years. The thick blue curve represents the cone of influence and the coherence above the 95% significance level is marked by the green contour. The ordinate is the period (days) plotted on a \log_2 scale. The horizontal lines from top to bottom mark 365, 180, 120, 90, and 30 days on the ordinate. The top panel shows the coherence between Mumbai and Goa, the second panel between Goa and Kollam, the third panel between Kollam and Kanyakumari, and the bottom panel between Mumbai and Kollam. The phase difference is shown by the arrows, which are marked only if the coherence exceeds 0.5. The current at the southern location leads (lags) the current at the northern location in anticlockwise (clockwise) direction.

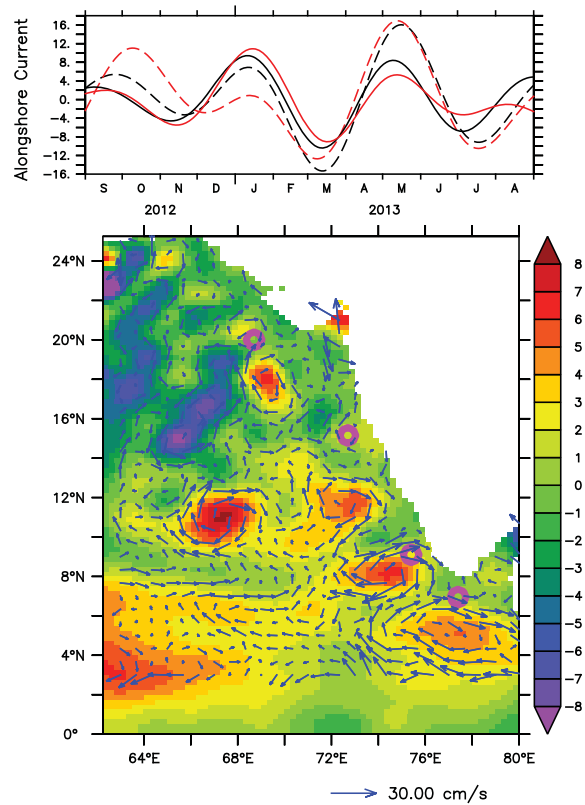


Figure 11: Intra-annual variability during 2012–2013 in the SEAS. The top panel shows the 100–250-day band-passed surface alongshore (solid curves) and cross-shore (dashed curves) current (cm s^{-1}) at the mooring location off Kollam. The black (red) curves are for the ADCP (OSCAR) data. The bottom panel is the SLA map, centred on 15 March 2013, overlaid with the OSCAR current vectors; both SLA and OSCAR current are filtered using a 100–250-days Lanczos filter. Note that the cross-shore component is much stronger than the alongshore component in mid-March 2013.

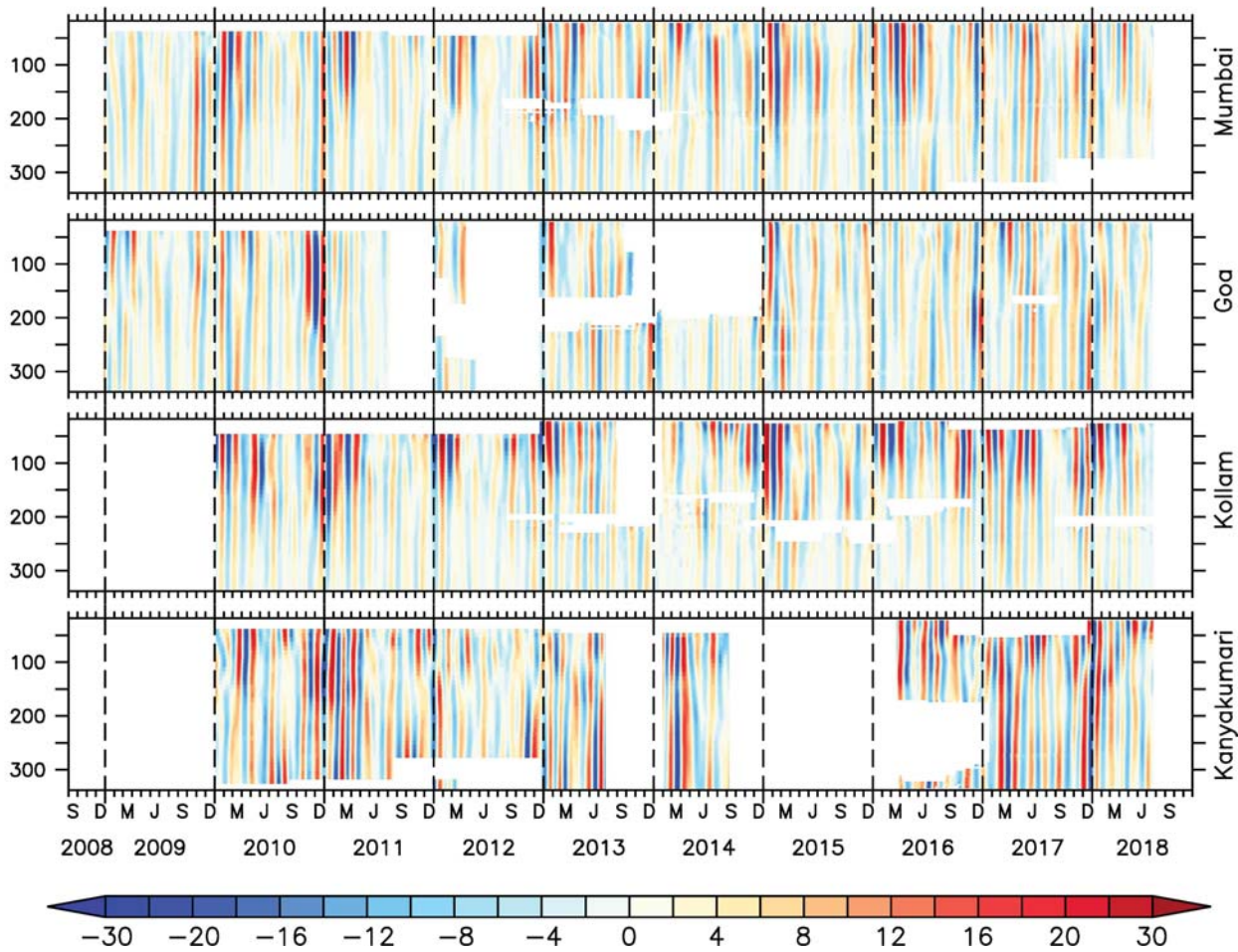


Figure 12: Intraseasonal (30–90-days band-pass-filtered) variability of the alongshore current (cm s^{-1}) at the four mooring locations. The vertical black dashed lines are used to separate the years. Strong intraseasonal variability is seen throughout the record and the variability in this band is stronger during the winter monsoon.

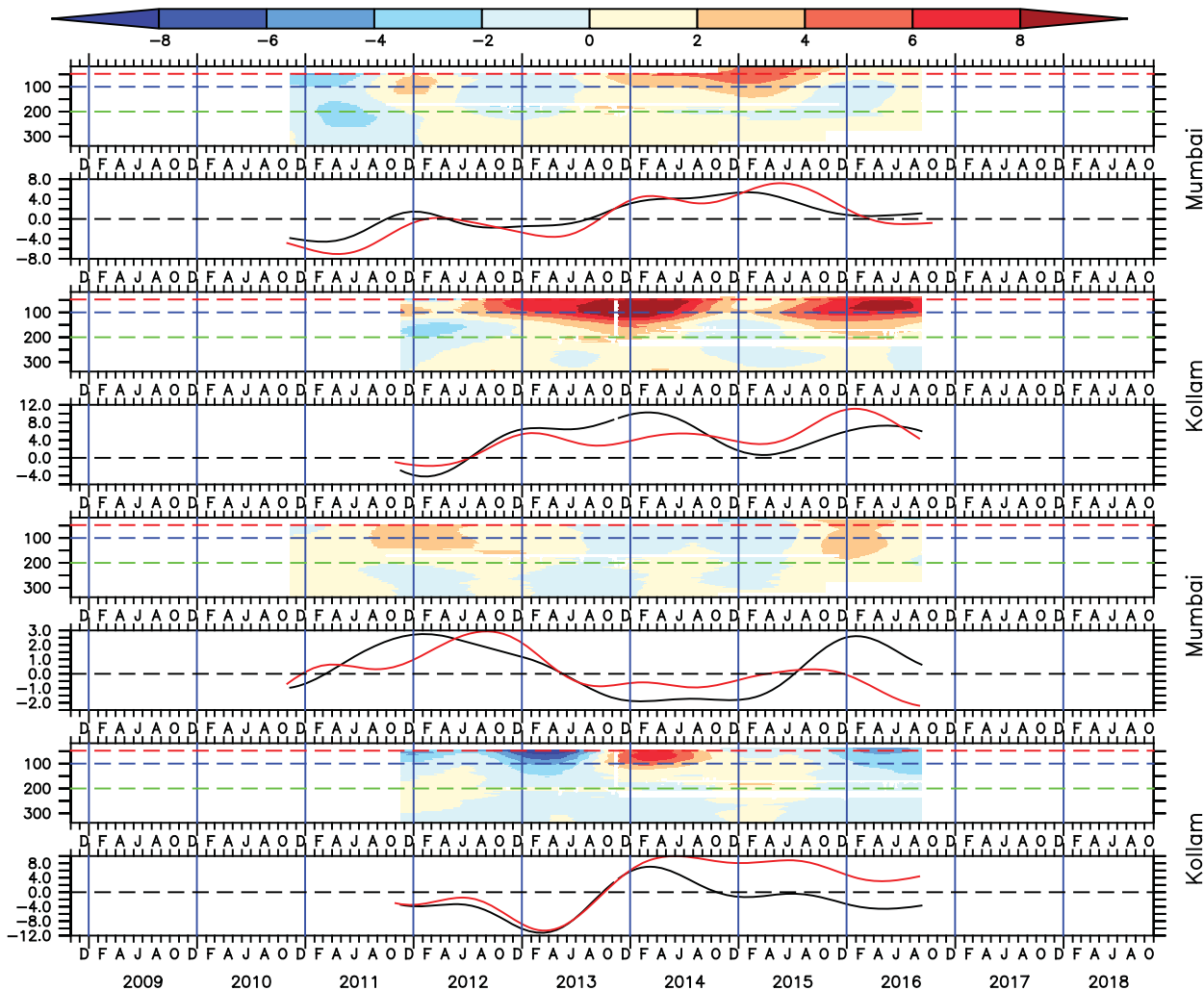


Figure 13: The sub-annual alongshore (AC) and cross-shore (CC) currents (in cm s^{-1}) obtained by applying a 500-day low-pass filter off Kollam and Mumbai. The vertical black dashed lines are used to separate the years. The odd panels show the sub-annual WICC as a function of time (abscissa) and depth (ordinate, m) and the even panels show the sub-annual current based on both ADCP (48 m, black) and OSCAR (red) data. The alongshore (cross-shore) component is plotted in the top (bottom) four panels. The sub-annual alongshore WICC is stronger than the annual alongshore WICC off Kollam; the sub-annual WICC is mostly poleward off Kollam. The cross-shore sub-annual current is also strong off Kollam.

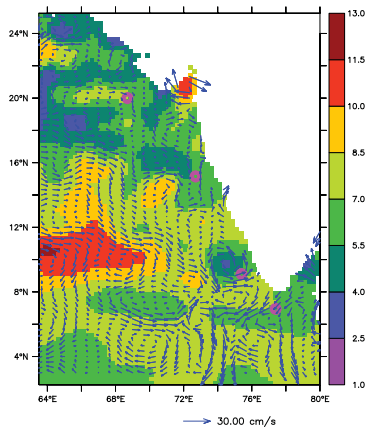


Figure 14: 500-day-low-passed AVISO SLA (cm) and OSCAR current (cm s^{-1}) on 28 February 2013.

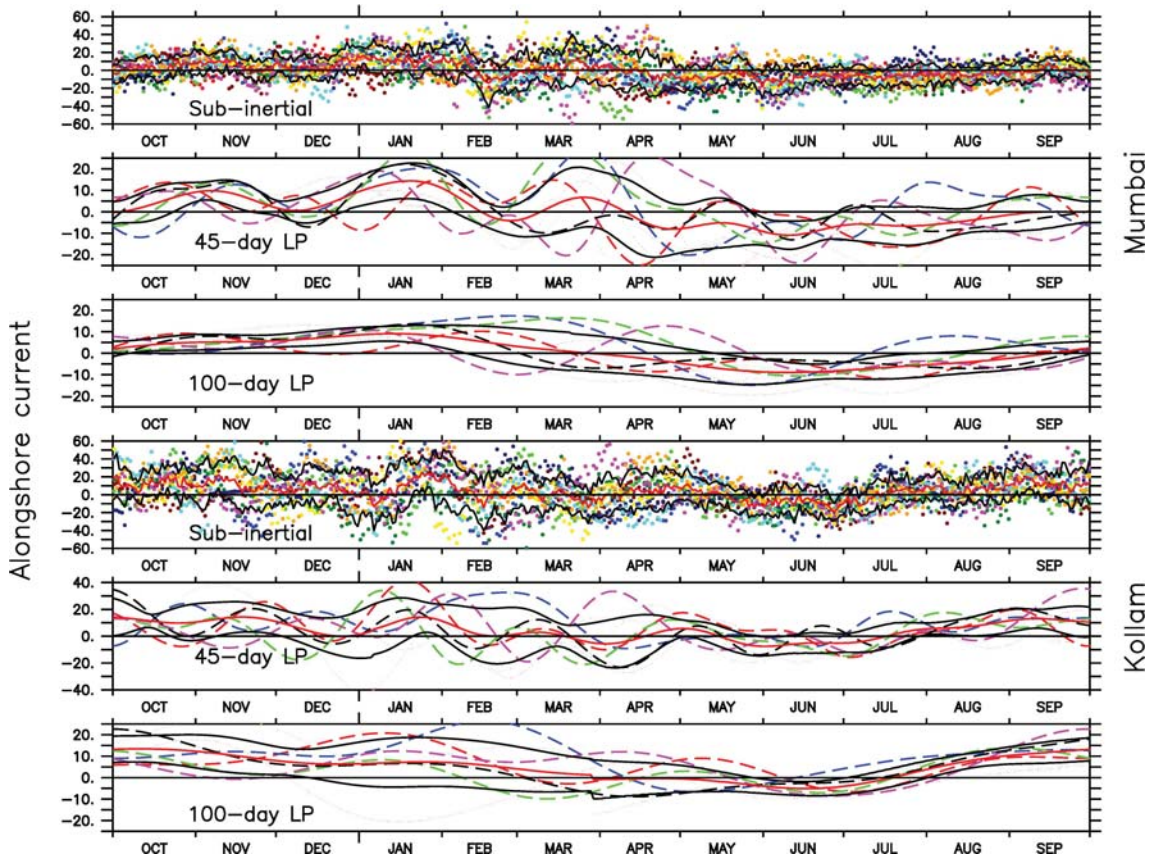


Figure 15: In which direction does the alongshore WICC flow on a given day? The first and fourth panels show the alongshore, sub-inertial WICC (cm s^{-1}) at 48 m off Mumbai (first panel) and Kollam (fourth panel). Positive values imply poleward flow. The solid black curve is the mean for the available data during 2009–2018 and each colour represents the current during a particular year. The dashed black curves mark one standard deviation about the mean. The second and fifth panels show the 45-day low-passed (LP) current off Mumbai (second panel) and Kollam (fifth panel); the Lanczos filter was used for filtering and the solid and dashed black curves and the coloured dots are as in the odd panels. Note the significant scatter of the coloured dots about the mean. The standard deviation is high and the zero line almost passes between the dashed curves over the entire year even for the 45-day low-passed current. Off Mumbai (Kollam), the zero line lies on one side of the curves only for part of November, January, and June (October, November, and September). That it is almost possible to draw a line between the curves representing one standard deviation shows the dominance of intraseasonal variability in the regime of the WICC. The third and sixth panels show the 100-day low-passed WICC off Mumbai (third panel) and Kollam (sixth panel); intraseasonal variability, defined in this paper as the variability in the 30–90-day band, is filtered out, leaving only the variability at higher periods. Therefore, the red curves in these panels represent the climatological seasonal cycle estimated from the ADCP data record. The mean seasonal current off Mumbai shows the canonical equatorward (poleward) flow during the summer (winter) monsoon, but the mean seasonal WICC is largely poleward off Kollam owing to the strong sub-annual flow (Fig. 13). The poleward WICC off Kollam reaches a magnitude of $\sim 15 \text{ cm s}^{-1}$ and the equatorward flow, which is restricted to May–July, is much weaker. The $1\text{-}\sigma$ curves in these panels represent the interannual variability, which is large at both locations.

